THE PENNSYLVANIA STATE UNIVERSITY
SCHREYER HONORS COLLEGE

DEPARTMENT OF BIOCHEMISTRY AND MOLECULAR BIOLOGY

# Mechanistic Study of Halogenation by Iron(II) and 2-Oxoglutarate-Dependent Oxygenases

BRYCE KATCH
SPRING 2022

A thesis
submitted in partial fulfillment
of the requirements
for baccalaureate degrees
in BMB (Biochemistry and Molecular Biology) and Chemical Engineering
with Honors in BMB (Biochemistry and Molecular Biology)

Reviewed and approved* by the following:

Amie K. Boal
Associate Professor of Chemistry and of Biochemistry and Molecular Biology
Thesis Supervisor

Timothy C. Meredith
Associate Professor of Biochemistry and Molecular Biology
Honors Advisor

* Electronic approvals are on file.

# ABSTRACT

Enzymes are responsible for catalyzing chemical reactions in living systems, making life as we know it possible. Many of the most challenging chemical reactions - reactions that involve breaking very stable bonds - are performed by enzymes that contain transition metals. The aliphatic carbon-hydrogen bond is an example of a bond that is typically considered inert; however, many enzymes in nature can make use of iron cofactors to activate this unreactive bond. One class of iron-dependent enzymes achieves C-H activation by coupling its chemistry to the oxidative decarboxylation of the small molecule 2-oxo-glutarate. This class of enzymes is known as the iron(II) and 2-oxo-glutarate-dependent (Fe/2OG) oxygenase superfamily. Here, we detail the study of two Fe/2OG enzymes- SadA and BesD- that perform halogenation of unactivated carbon-hydrogen bonds. SadA is a hydroxylase enzyme that we engineered to install a halide on an amino-acid derivative substrate, while BesD is natively a halogenase of a lysine substrate. Our work demonstrates that the reactivity of these enzymes can be expanded beyond their primary activity through mutagenesis or reaction with alternative substrates. We also show that these enzymes display creative strategies to favor the halogenation reaction over the canonical hydroxylation reaction. This work furthers our understanding of enzymatic C-H activation and showcases the potential biocatalytic value of this enzyme superfamily.

# TABLE OF CONTENTS

# LIST OF FIGURES

# LIST OF TABLES

## ACKNOWLEDGEMENTS

I would first like to thank Pedro Rivera-Pomales, who served as my mentor during my initial two years in the lab working on the SadA project. I would also like to thank my mentors during my final year, Jeff Slater and Laura Collazo-Perez. Pedro, Jeff, and Laura- all your efforts and assistance in lab have transformed the way I look at science and will continue to shape how I approach research in the future. I hope you know how much I truly appreciate your time and mentorship. Lastly, I would like to thank Dr. Amie Boal for allowing me to do work in her lab and for her help in writing this thesis. Your advice and guidance throughout the past 3 years has been invaluable; I am so grateful to have started off my scientific research journey in such a fantastic lab.

# Chapter 1

## Background on iron(II) and 2-oxoglutarate dependent oxygenases

## Introduction

Iron(II) and 2-oxoglutarate dependent oxygenase (Fe(II)/2OG) enzymes represent a staggeringly diverse family of biological catalysts capable of performing a wide range of chemical transformations. The enzyme family is linked by the use of a mononuclear iron(II) cofactor and a 2-oxoglutarate co-substrate to cleave chemically inert $sp^3$ carbon-hydrogen bonds.[1] The chemical reactions catalyzed by these enzymes have garnered scientific interest due to both their chemical and biological relevance. From a synthetic chemistry perspective, the current non-enzymatic approaches to $sp^3$ C-H functionalization lack specificity, leading to the formation of unwanted byproducts, and require the use of environmentally hazardous catalysts and solvents.[2] In contrast, iron(II) and 2-oxoglutarate enzymes offer exquisite specificity in mild aqueous conditions, demonstrating promise as potential biocatalysts.[3] Furthermore, since 2-oxoglutarate (also known as alpha-ketoglutarate) is a central metabolite found in the citric acid cycle, biocatalytic usage of these enzymes in living cells or cell extracts would be feasible. Fe(II)/2OG enzymes also play a central biological role in nearly all living organisms. Fe(II)/2OG enzymes have been implicated in a variety of critical biological processes including the modification of DNA, histone proteins, and ribosomes, among others.[4] Fe(II)/2OG enzymes also play a key role in microbial biosynthetic pathways; it is in these pathways in which the most diverse chemistry has been observed.[4] Overall, the chemical and biological importance of Fe(II)/2OG enzymes motivates investigation into their function.

## Diverse reactivity among iron(II) and 2-oxoglutarate dependent oxygenases

Though all Fe(II)/2OG enzymes use common cofactors to perform chemistry, a diversity of reaction outcomes have been observed. Most characterized Fe(II)/2OG enzymes follow a similar mechanistic route to form a high valent iron(IV)-oxo species, also known as a ferryl. The ferryl intermediate is responsible for abstraction of a hydrogen from an aliphatic substrate carbon. Following hydrogen abstraction, the mechanisms diverge based on reaction outcome.[5]

Most of the characterized Fe(II)/2OG enzymes perform hydroxylation.[4] Furthermore, of the Fe(II)/2OG enzymes relevant to human health, nearly all are hydroxylases.[4] For example, the ten-eleven translocation (TET) methylcytosine dioxygenases catalyze several of the reactions required to reverse cytosine methylation, a process associated with gene silencing and heterochromatin formation.[6] TET1 performs the first reaction in cytosine demethylation in which the methyl group is hydroxylated to form 5-hydroxymethylcytosine. Hypoxia-inducible factor prolyl hydroxylase (HIF-PH) represents another biologically relevant Fe(II)/2OG enzyme that installs a hydroxyl group on the 4-carbon of proline; it acts on hypoxia inducible factor (HIF) to signal low oxygen levels, effectively acting as an oxygen sensor.[7] Compared to these examples in human biology, however, when it comes to studying the biochemical mechanism — of all the known Fe(II)/2OG hydroxylases, the microbial, taurine-degrading enzyme TauD may be the most well-characterized, serving as a "model" hydroxylase in terms of mechanism (Figure 1).[8] Analogously, when it comes to structure, the enzyme VioC serves as the model hydroxylase as structures have been solved for many of its fleeting intermediates.[9]

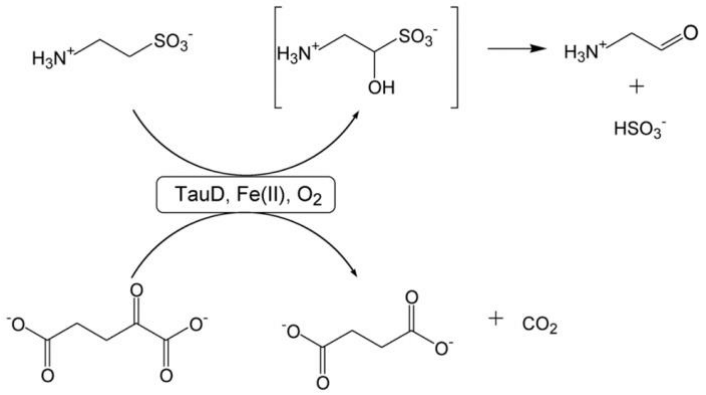


**Figure 1. TauD reaction scheme.** TauD is an archetypal Fe(II)/2OG hydroxylase; the enzyme hydroxylates taurine, leading to its degradation.[8] Like most Fe(II)/2OG enzymes, it uses an iron cofactor, 2-oxoglutarate co-substrate, and molecular oxygen to functionalize an aliphatic carbon-hydrogen bond.

Aside from hydroxylation, Fe(II)/2OG enzymes are capable of installing other functional groups onto aliphatic carbons. Several enzymes use hydroxylation as a first step but perform an additional turnover to further transform the substrate. For example, the enzyme LolO performs hydroxylation followed by cyclization to yield an oxacyclic product. Similarly, the enzyme H6H forms an epoxide by performing hydroxylation and epoxidation in sequence.[11] Other observed outcomes in Fe(II)/2OG enzymes include stereoinversion, desaturation, and halogenation.[5]

Among these alternate transformations, halogenation is of particular scientific interest— Fe(II)/2OG halogenases show promise in biocatalytic roles, as selective halogenation at aliphatic centers is useful both as a synthetic tool and as a way to modulate bioactivity of small molecules.[12] The recent discovery of BesD, which chlorinates the amino acid L-lysine, is of special note (Figure 2).[12] Previously reported Fe(II)/2OG halogenases either required the use of a large carrier protein to deliver the substrate (i.e. SyrB2) or accepted large, functionally-dense substrates (i.e. WelO5), making enzymatic characterization and biocatalytic application challenging.[13,14] The relevance of halogenation motivates the work for this thesis in both designing a halogenase enzyme from the hydroxylase, SadA, and further characterizing the substrate scope and properties of native halogenase, BesD.

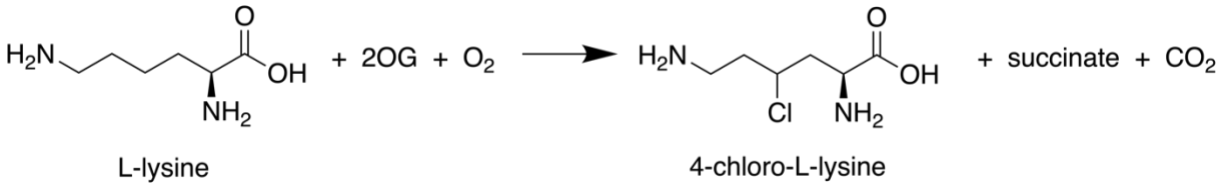


**Figure 2. BesD reaction scheme.** BesD is an Fe(II)/2OG halogenase enzyme that installs a chloride at the 4-carbon of L-lysine to form 4-chloro-L-lysine. The halogenation reaction, like the canonical hydroxylation reaction, is linked to oxidative decarboxylation of the 2-oxo-glutarate co-substrate.

## Iron(II) and 2-oxoglutarate dependent oxygenase structure and mechanism

Fe(II)/2OG enzymes are capable of achieving a wide range of reaction outcomes with a simple and highly conserved structure. Based on crystallographic studies, the active site is located in a double-stranded beta-helix fold (also known as the jelly-roll or cupin). In the active site, the central Fe(II) is coordinated by two histidine residues and one carboxylate moiety from either aspartate or glutamate (Figure 3). These three residues are highly conserved among Fe(II)/2OG enzymes and are known as the facial triad.[1] The notable exception to this rule is in the Fe(II)/2OG halogenase enzymes; in these systems, the aspartate or glutamate residue is replaced with a less occlusive alanine or glycine to accommodate a halide coordinating to the iron.[14]

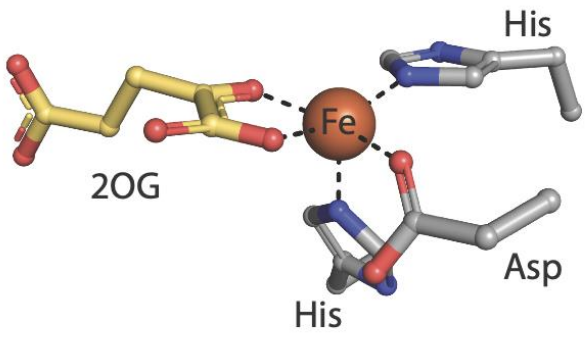


**Figure 3. Active site of an Fe(II)/2OG hydroxylase.** Fe(II)/2OG hydroxylases coordinate iron with two histidine residues and either an aspartate or glutamate residue. 2OG binds bidentate to the iron cofactor.[15]

Of all Fe(II)/2OG-catalyzed reactions, the hydroxylation mechanism is best understood and thus serves as a starting point for mechanistic discussion (Figure 4). At the beginning of the hydroxylation reaction cycle, iron(II) is coordinated to the facial triad with three water molecules occupying the empty coordination sites.[15] Next, 2-oxoglutarate coordinates bidentate to the iron through both the carboxylate and ketone functional groups, displacing two water molecules.[16] The substrate can then bind, displacing the final water molecule. Following formation of this quaternary complex, oxygen adds to the iron(II) to form an iron(III)-superoxo species. The oxygen atom distal to the iron then attacks the 2-carbon of 2-oxoglutarate in a decarboxylation reaction, forming succinate bound to an iron(IV)-oxo (ferryl) species.[17,18,19] The ferryl abstracts a hydrogen from the substrate, forming a carbon radical.[20] The resulting Fe(III)-OH donates the OH to the carbon radical, forming a hydroxylated product.[21] The hydroxylated product and succinate diffuse from the active site and are replaced by three water molecules, returning the active site to the beginning of the reaction cycle.[5]

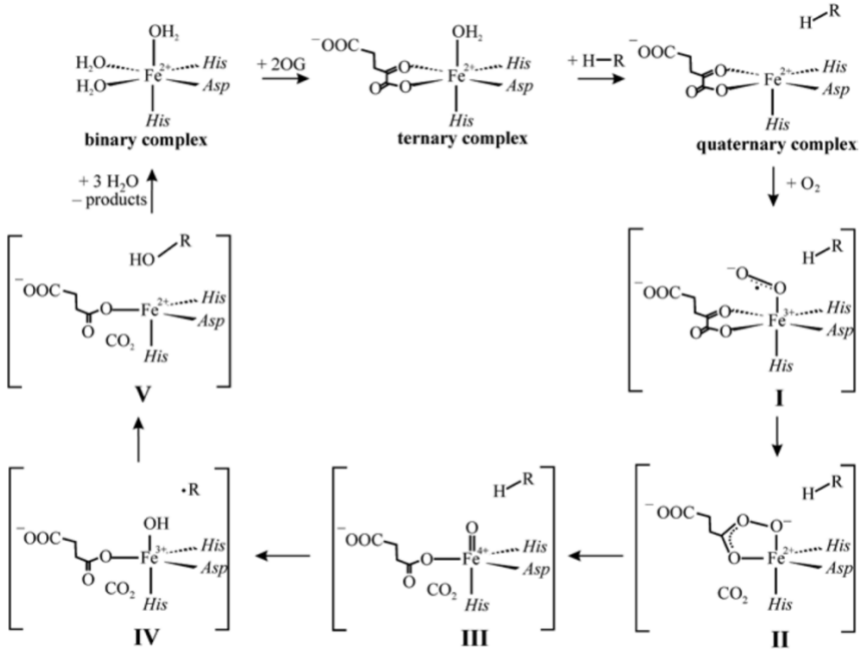


**Figure 4. Consensus Fe(II)/2OG hydroxylation mechanism.** Fe(II)/2OG hydroxylases have a conserved mechanism; Fe(II)/2OG enzymes with alternate reaction outcomes often follow the same steps up until formation of intermediate (IV) which serves as a branch point.[5]

Proposed halogenation mechanisms parallel the consensus hydroxylation mechanisms, with several distinctions to facilitate the addition of a halide rather than a hydroxyl. Halide addition is understood to occur following hydrogen abstraction while Fe(III) remains coordinated to the hydroxyl, known as the alternate group transfer mechanism.[5] To enable this reaction, a glycine or aspartate replaces the carboxylate residue, allowing for direct coordination of a halide with the metal cofactor.[1] Additionally, halogenases generally employ some strategy to favor addition of a halide over addition of a hydroxyl. In the halogenase SyrB2, researchers have put forth a substrate positioning hypothesis, in which if a carbon center resides nearest the Fe(III)-OH moiety, it will be hydroxylated, while if nearer to the halide, it will be halogenated.[5] The first structure of an Fe/2OG halogenase (WelO5) in complex with its substrate corroborated some aspects of this proposed mechanism but also revealed some surprising features.[14] In the characterized quaternary complex (iron(II), 2OG, substrate, and chloride), the targeted carbon resides nearer where the expected Fe(III)-OH would be rather than the chloride. This result alone seemingly opposes the substrate positioning hypothesis, given that the target carbon is nearer the expected -OH rather than -Cl yet still favors halogenation over hydroxylation. However, since halogenation is observed, it is proposed that the oxo unit of the ferryl intermediate is repositioned away from the target carbon, potentially orchestrated by hydrogen bonding with a serine (S189) and perhaps also with the succinate carboxylate group.[14] With the discovery and characterization of BesD, there appear to be additional avenues through which Fe(II)/2OG halogenases can achieve selective halogenation. In BesD, the 2OG co-substrate binds initially in an orientation that would suggest that molecular oxygen can add in the location that the oxo ligand in WelO5 ultimately migrates to, avoiding the need for ligand rearrangement (Figure 5).[12]

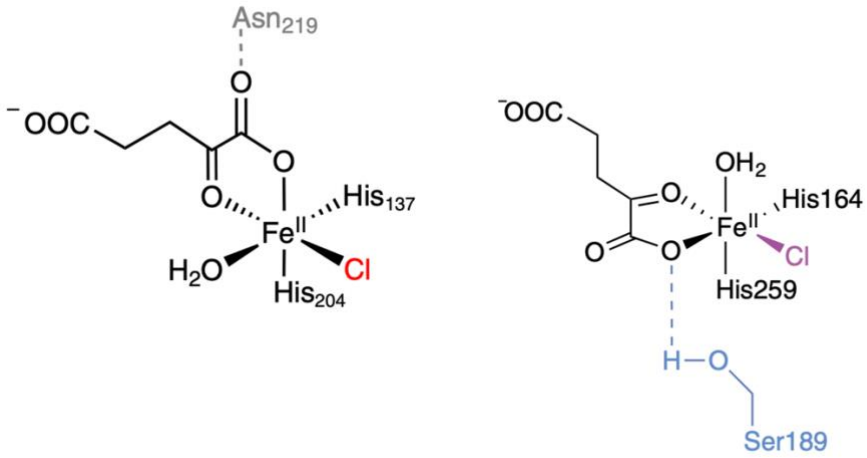


**Figure 5. Comparison of quaternary complexes in BesD (left) and WelO5 (right).** The 2OG co-substrate in BesD binds with the carboxylate oxygen coordinated in the axial plane, potentially allowing molecular oxygen to bind trans to His-137 and avoid ferryl rearrangement.[12] In WelO5, the oxygen binds trans to His-259, which requires the oxo ligand to migrate into the equatorial plane to repress hydroxyl rebound.[14]

Overall, the mechanistic novelty of Fe/2OG halogenases and the utility of their halogenated products motivates continued investigation into these systems. Thus, the work presented in this thesis revolves around the halogenation reaction, how it is controlled, and how it can be altered. We first focus on the native hydroxylase SadA, and we demonstrate that structure-guided amino acid substitutions can be made to introduce halogenation reactivity. This work has implications in biocatalysis and exemplifies the chemical versatility inherent to the Fe(II)/2OG superfamily. Then, we discuss the recently discovered native halogenase BesD and probe its mechanism with kinetic and spectroscopic studies. We report unexpected mechanistic features of this enzyme, demonstrating that the chloride ion occupying the active site plays a key role in substrate binding and reaction outcome. Between SadA and BesD, it becomes evident that the non-canonical halogenation reaction involves an added degree of complexity not seen in most hydroxylase systems to successfully carry out installation of a halide.

# Chapter 2

## Introducing halogenation reactivity into the hydroxylase, SadA

## Introduction

When considering biocatalytic applications for halogenation, simplicity and flexibility of the enzyme system are of primary interest. Many Fe(II)/2OG halogenases target complex substrates, limiting the extent of both scientific investigation and biocatalytic application. Two of the better-characterized halogenases fall under this category. The enzyme SyrB2, which formed the basis of substrate positioning arguments in Fe(II)/2OG halogenases, uses a carrier protein (SyrB1) to deliver its substrate.[13] The use of a carrier protein not only complicates experimental study but is not ideal for a scaled-up biocatalytic system. Similarly, WelO5, which is perhaps the best structurally-characterized halogenase, utilizes a complex and functionally dense substrate that is expensive to synthesize.[14] Thus, there is interest in expanding the pool of Fe(II)/2OG halogenases that act on simple, synthetically useful, substrates. This notion formed the basis of initial efforts with the enzyme SadA.

Given that Fe(II)/2OG hydroxylases and halogenases share cofactors in addition to similar structural features, Mitchell et. al. sought to take a hydroxylase and mutate the active site to introduce halogenation capability.[22] They selected the hydroxylase SadA as it shares high structural similarity to WelO5, a known halogenase. Natively, SadA accepts N-succinyl-L-leucine as a substrate and hydroxylates the beta carbon (Figure 6). By converting SadA into a halogenase, it would install a chloride or bromide at the same carbon center. There is also interest in testing for azidation activity, or installation of an $N_3$ anion, which has demonstrated to be a synthetically useful intermediate, particularly in click chemistry.[23,24]

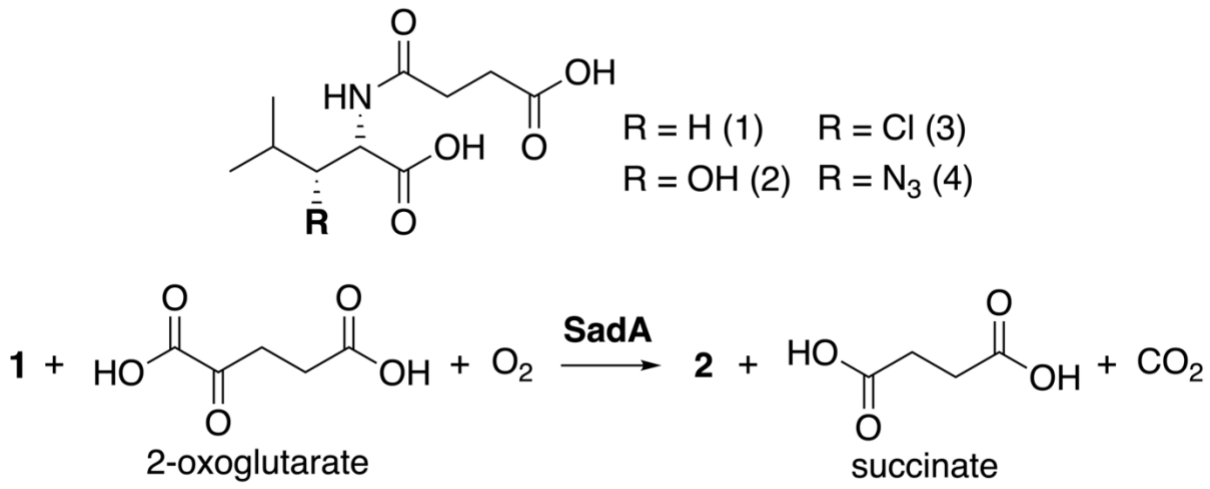


**Figure 6. SadA reaction scheme.** Natively, SadA functionalizes the C-H bond (1) of N-succinyl-L-leucine with a hydroxyl (2). Through structure-guided mutagenesis, SadA can install a chloride (3) or azide (4).

Comparison of the active sites of wild type SadA (A) with WelO5 (B) demonstrates distinctions between hydroxylase and halogenase structure (Figure 7). SadA exhibits the facial triad (His-X-Asp-$X_n$-His), while WelO5 has a glycine substituted in place of the aspartate.[14,22] Additionally, the chloride in WelO5 coordinates iron in place of the carboxylate provided by the aspartate residue. By examination of these structures, Mitchell et. al. substituted the aspartate for glycine, which afforded some halogenation reactivity. However, even after this substitution, hydroxylated product still exceeded halogenated product, and the efficiency of the catalytic cycle also decreased, with unproductive Fe(II) oxidation observed.[22] These preliminary results set the ground work for further exploration of SadA mutagenesis. One key aim was to further explore the substrate scope of SadA to determine the range of substrates that SadA could theoretically halogenate. Additionally, exploring the structural basis for altered reactivity was a goal to further understand the means by which Fe(II)/2OG enzymes halogenate substrate.

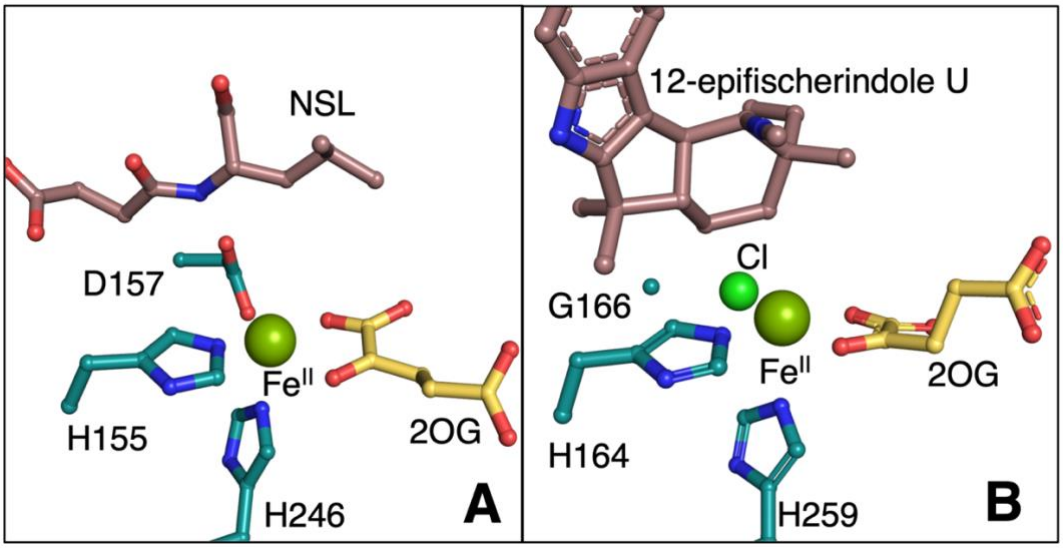


**Figure 7. Side-by-side comparison of SadA and WelO5 active sites.** (A) SadA contains the His-X-Asp/Glu-$X_N$-His motif conserves in Fe(II)/2OG hydroxylases.[22] (B) WelO5 substitutes the carboxylate-supplying reside for a glycine, allowing for coordinate of a halide to the iron cofactor.[14]

## Results and Discussion

### LC-MS Assays with SadA D157G and D157S Variant Enzymes

To test for halogenation capacity, activity assays were performed with wild type SadA, glycine-substituted SadA (D157G), and serine-substituted SadA (D157S) (Figure 8). With the native substrate, N-succinyl-L-leucine (NSL), the wild type enzyme converts nearly all substrate to hydroxylated product, consistent with previous characterization efforts. In the glycine variant, nearly all substrate is also converted— chlorinated product is detected, though the majority of product is hydroxylated. This result is also consistent with the SadA data published by Mitchell et. al. regarding the glycine substitution.[22] An additional substitution, aspartate to serine, was tested. This enzyme produces a superior halogenation/hydroxylation ratio relative to the glycine variant; however, there is also a decrease in enzymatic efficiency suggested by unconverted substrate.

The same activity assays were then performed with an alternate substrate, N-succinyl-isoleucine (NSI), to test substrate scope of the enzyme. Like with N-succinyl-L-leucine, the wild type consumed all substrate and performs 100% hydroxylation. The glycine variant with N-succinyl-isoleucine follows the same pattern as with N-succinyl-L-isoleucine, with complete consumption; some halogenated product is detected, though most is hydroxylated. Lastly, the serine variant consumes most but not all of N-succinyl-L-isoleucine. Interestingly, it does produce more chlorinated product than hydroxylated.

Beyond the scope of halogenation, we sought to test the ability of SadA to azidate substrate. The same set of assays used to test for halogenation was repeated but with the presence of azide anions (Figure 9). The results of the azide assays were consistent with those of the chloride; the wild type exclusively hydroxylates, while glycine and serine variants show azidation activity. Interestingly, the D157S variant produces two distinct azidated N-succinyl-L-isoleucine products, suggesting reactivity on two different carbons. Like with the chloride assays, the serine variant shows a greater preference for the alternate reaction relative to hydroxylation, but the hydroxylation still is the dominant outcome.

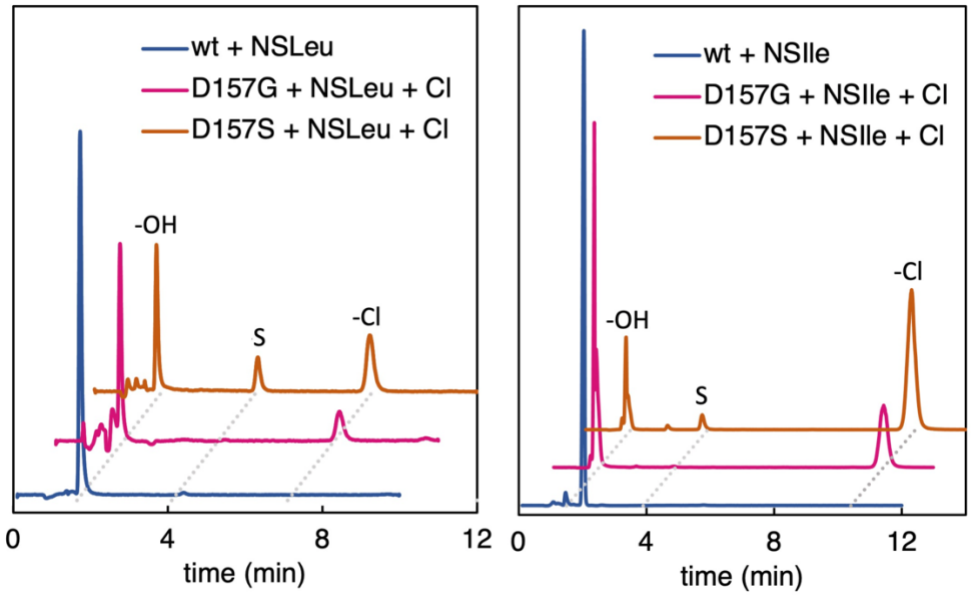


**Figure 8. Total ion chromatograms detecting chloride installation.** Both D157G and D157S enzymes exhibit halogenation reactivity, though hydroxylation remains a dominant outcome.

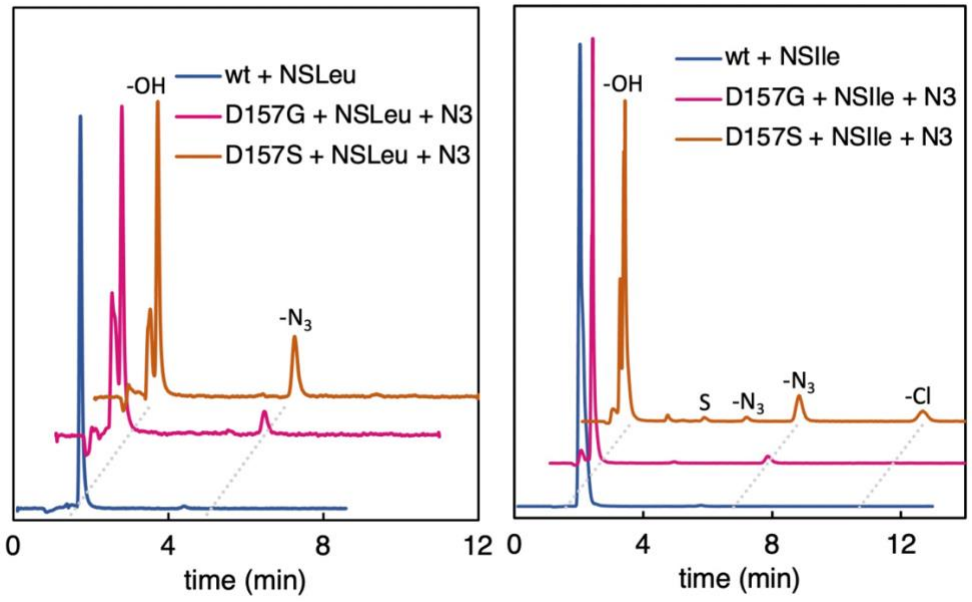


**Figure 9. Total ion chromatograms detecting azide installation.** Both D157G and D157S enzymes exhibit some azidation reactivity. D157S produces two distinct azidated NSIle products.

Because the D157S variant showed the poorest substrate consumption, the coupling of substrate consumption to substrate consumption was assayed. A perfect Fe(II)/2OG enzyme would exhibit a 1:1 ratio between substrate consumed and succinate produced. However, in an imperfect, decoupled enzyme, succinate production can occur while leaving the substrate unreacted. When coupling was tested for the chloride assays, the reaction with NSL exhibited approximately 63% coupling (a perfectly coupled enzyme running at 100%), suggesting unproductive oxidation (Figure 10). This result is consistent with unconverted substrate in the activity assay. The NSI reaction was better coupled, at around 94%, which is reflected in a higher degree of substrate consumption in the activity assay. Coupling for azidation reactivity was also tested; both reactions with NSL and NSI yielded 94%, consistent with the nearly complete substrate consumption in both activity assays (Figure 11).

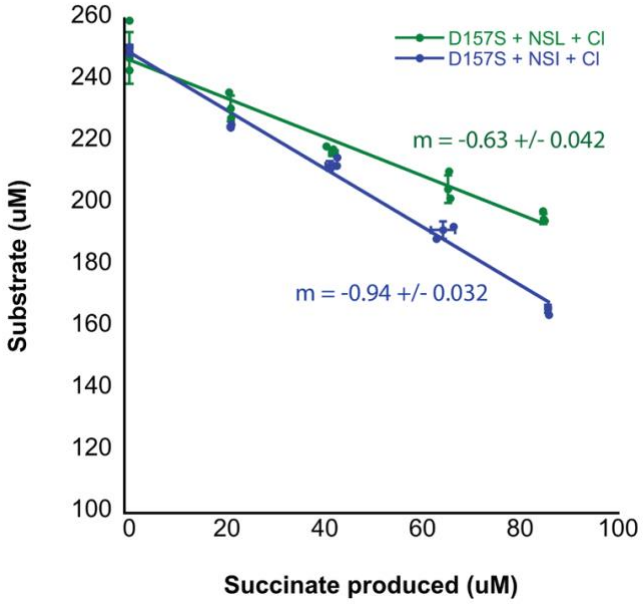


**Figure 10. Coupling of succinate production with substrate consumption for chlorination.** The reaction with NSL exhibits unproductive oxidation in ~37% of catalytic turnovers, while the reaction with NSI is well-coupled at ~94%.

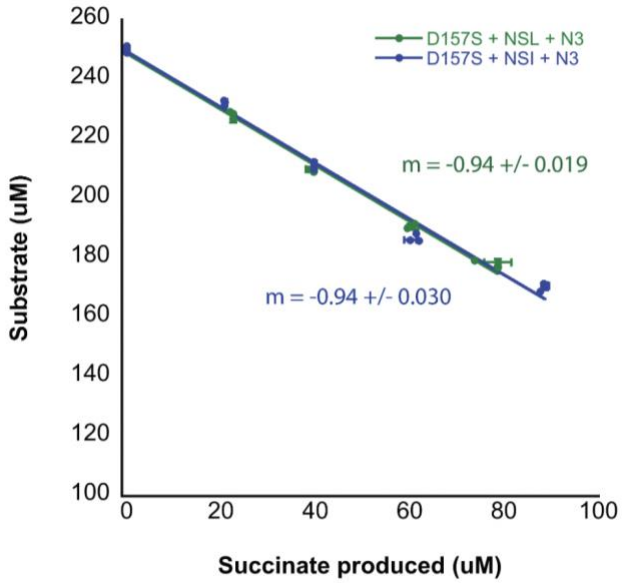


**Figure 11. Coupling of succinate production with substrate consumption for azidation.** The azidation of both NSL and NSI is well-coupled, with ~94% of succinate production tied to substrate consumption for both reactions.

## Crystal Structures of SadA D157G and D157S Variant Enzymes

To assess the structural basis for reactivity in the SadA variant enzymes, crystal structures were obtained for SadA D157S in complex with NSL and SadA D157G in complex with NSI (Figure 12). Although a crystal structure could not be obtained for each enzyme/substrate combination assayed, the structures shed light on differences in reactivity by showing substrate positioning of the target carbon. For the serine variant, the substrate target carbon is shifted spatially relative to the wild type complex. With the carbon nearer the succinate ligand; a WelO5-like rearrangement may facilitate halogenation in this instance with the oxo ligand migrating to minimize OH rebound. However, based on the activity assay data, hydroxylation and halogenation occur in similar amounts, possibly suggesting a lower efficiency at which the variant enzyme can suppress hydroxylation. Thus, even if this rearrangement does occur, it is likely not geometrically optimized to favor halogenation. The chloride ligand is visualized in the structure of the glycine variant; here, a similar rearrangement may occur to facilitate chlorination of the beta carbon. Like the serine variant, the glycine variant retains significant hydroxylation activity, again demonstrating that the enzyme cannot efficiently suppress all hydroxylation. We also determined two structures with alternative substrate isoleucine. Here, both the beta and gamma carbons of the substrate side chain reside sufficiently close to the iron center to react, possibly explaining the presence of two distinct azidation products. Overall, the crystal structures support the reactivity observed through the substrate positioning hypothesis.

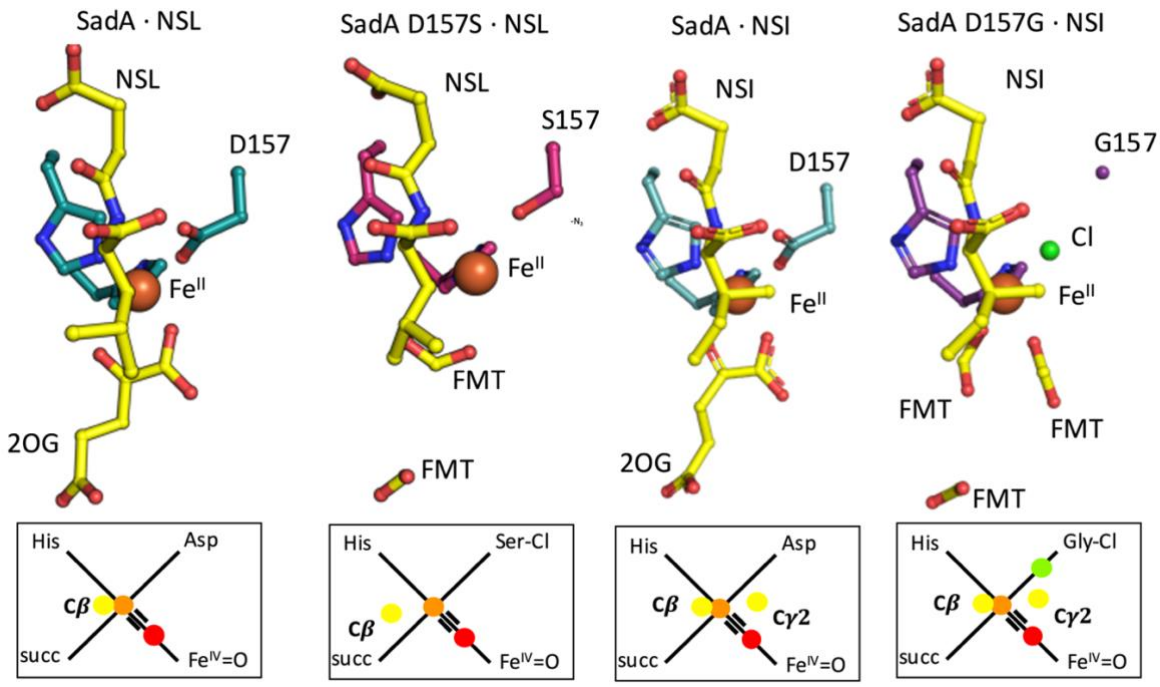


**Figure 12. Crystal structures of wild type SadA, D157S, and D157G.** Two-dimensional projection of proposed substrate orientation with respect to reactive iron (IV) species (lower). Position of reactive substrate carbons (yellow) are shown relative to iron(IV) (orange), oxo (red), and chloride (green).

## Discussion and Broader Impacts

SadA is an example of how an enzymatic scaffold can be modified to generate a variety of reaction outcomes with a reasonable range of substrates. We show that based on mechanistic knowledge of enzymatic halogenation, we can introduce seemingly disparate reactivity into an enzyme that performs the canonical Fe(II)/2OG enzyme reaction, hydroxylation. Because hydroxylases represent the bulk of characterized Fe(II)/2OG enzymes, this chapter lays the groundwork for how these enzymes could be repurposed to afford synthetically useful products. Furthermore, given the active site conservation shared by hydroxylases and halogenases, substitution of the carboxylate for an alanine/glycine could theoretically enable halogenation in a wide variety of Fe(II)/2OG hydroxylases.

Though SadA demonstrates the potential of Fe(II)/2OG hydroxylases to be reprogrammed, it also demonstrates many limitations inherent to rational protein engineering. While the desired reactivity was observed in the SadA mutants, the selectivity for halogenation and azidation was not ideal. In all assays conducted, hydroxylated product was still detected (and in many cases exceeded the preferred product), indicating that the single amino acid substitution is generally not sufficient to rival the activity of a native halogenase. Though additional informed mutations could be made, it is often very challenging to predict the effect a single mutation will have on the protein's structure and activity. While they are not documented in this thesis, several additional mutations to improve selectivity were attempted; some substitutions afforded slightly improved selectivity, while others deactivated the enzyme altogether.

In light of the challenges associated with rational protein design, evolution-based methods are becoming increasingly dominant when it comes to affording a truly useful biocatalyst.[25,26] To recapitulate reactivity that is comparable to a native halogenase, it may be most efficient to evolve the singly-substituted SadA iteratively using high-throughput screening methods. Several reports of evolved Fe(II)/2OG enzymes have been reported in the literature, demonstrating methods that could be applied to the SadA project.[27,28] In a recently published paper in Nature Chemical Biology, Neugebauer et. al. detail the conversion of a Fe(II)/2OG lysine hydroxylase into a halogenase through screening of randomly generated "shuffle libraries"— the researchers randomly shuffled and combined segments from the genes for hydroxylase and halogenase enzymes to generate chimeric protein genes that were expressed and assayed.[28] The creation of these chimeric proteins ultimately yielded a protein that has halogenation activity and selectivity comparable to its native halogenase counterpart.[28] Highlighting challenges associated with rational design, many of the key residues required for halogenation outlined in this paper reside in the second-sphere, which often may have unpredictable roles in controlling enzymatic activity.

Above all, these efforts, whether by rational design or by random library generation, highlight the beauty and simplicity of the Fe(II)/2OG system. Despite using the same cofactors and sharing a highly conserved active site, these enzymes perform a remarkable range of chemical transformations. Fe(II)/2OG

enzymes achieve this diversity of chemical reactivity by carefully orchestrating their active site to perform their desired function in often unpredictable ways. In the relatively small range of characterized native and engineered Fe(II)/2OG halogenases, we have seen that these enzymes employ different and creative strategies to favor the installation of a halide rather than the canonical hydroxyl functionalization. Further structural and mechanistic investigation of Fe(II)/2OG halogenation will continue to shed light on these interesting and perplexing systems.

## Materials and Methods

*SadA cloning, overexpression, and purification.*

SadA variants were generated and purified using procedures reported previously by Mitchell and colleagues.[22]

*LC-MS activity assays*.

50 $\mu$L reactions containing 100 mM HEPES pH 7.5, 100 $\mu$M enzyme, 100 mM ferrous ammonium sulfate, 2 mM 2OG, 1 mM substrate, 5 mM ascorbate, 1 mM tryptophan, and 50 mM NaCl/$NaN_3$ were prepared under anaerobic conditions. Following preparation and mixing of the solutions, the reactions were removed from the anaerobic chamber and mixed with 50 $\mu$L cold, air saturated buffer (~0.18 mM $O_2$). The reaction was allowed to proceed for 3 hr at room temperature. After 3 hr, the reaction products were isolated with 10k MWCO spin filter tubes at 14000 XG for 10 min (Pall). A mobile phase of 85:15 1% formic acid: acetonitrile was used for isocratic elution on a Zorbax Extended C-18 column attached to an Agilent 1200 Series HPLC; product detection analysis was then performed with an Agilent 6410 Triple Quad LC-MS. Chromatographs were analyzed with MassHunter software, and plots were generated with KaleidaGraph.

*Substrate/succinate coupling assays*.

Reactions containing 50 mM HEPES pH 7.5, 250 $\mu$M enzyme, 200 $\mu$M ferrous ammonium sulfate, 0-160 $\mu$M 2OG, 500 $\mu$M substrate, 250 $\mu$M d4-succinate, 1 mM tryptophan, and 50 mM NaCl/$NaN_3$ were prepared anaerobically. The reaction mixtures were removed from the anaerobic chamber and mixed with an equal volume of cold, air-saturated buffer. Following a 15-min incubation, the reaction was quenched with formic acid; the reaction products were with 10k MWCO spin filter tubes at 14000 XG for 10 min (Pall). A mobile phase of 85:15 1% formic acid: acetonitrile was used for isocratic elution on a Zorbax Extended C-18 column attached to an Agilent 1200 Series HPLC; product detection analysis was then performed with an Agilent 6410 Triple Quad LC-MS. Chromatographs were analyzed with MassHunter software, and plots were generated with KaleidaGraph.

*Crystallographic methods.*

X-ray diffraction data was collected at the Advanced Photon Source (APS) LS-CAT and GM-CAT beamlines. Diffraction data was processed using HKL2000 software. Molecular replacement was performed using previously published SadA coordinates (PDB 3W21) as the initial search model in CCP4 PHASER. Model building and refinement was performed in COOT and CCP4 Refmac5. NSL coordinates and restraints were generated with JLigand, and NSI coordinates and restraints were generated with PRODRG. Phenix software was used for a final round of refinement. The Molprobity server was used to validate coordinates and perform Ramachandran analysis.

*SadA • 2OG • NSL • Fe(II)*

Protein solution was prepared anaerobically with 10 mg/mL enzyme, 1 eq. ferrous ammonium sulfate, 5 eq. 2OG, and 1 eq. NSL. Reservoir solution was prepared with 0.1 M MES pH 6.5, 3 M sodium formate, and 0.05 M praseodymium (III) acetate. Protein and reservoir solution was mixed 1:1 on a coverslip and allowed to equilibrate with the reservoir solution via the hanging drop vapor diffusion method. Diamond-shaped crystals appeared in 1 d. The crystals were soaked in a solution of 0.1 M MES pH 6.5 and 1 mM 2OG for 30-60 min prior to being placed in a cryoprotectant solution containing 0.1 M

MES pH 6.5, 1 mM 2OG, and 20% glycerol and flash-frozen with liquid nitrogen. Crystals diffracted in the $P32_1$ space-group with four monomers in the asymmetric unit. The final model contains residues 1-273 in chain A, 1-273 in chain B, 1-273 in chain C plus His tag, 1-273 in chain D plus His tag, 5 Fe(II) atoms, 4 2OG molecules, 4 NSL molecules, and 56 water molecules. 97.73% of modeled residues are Ramachandran-preferred or allowed. No rotamer outliers are in the final model. An overall clash score of 6.89 is reported for the final model (Molprobity).

*SadA• 2OG • NSI • Fe(II)*

Protein solution was prepared anaerobically with 10 mg/mL enzyme, 1 eq. ferrous ammonium sulfate, 5 eq. 2OG, and 1 eq. NSI. Reservoir solution was prepared with 0.1 M MES pH 6.5, 3.5 M sodium formate, and 0.05 M praseodymium (III) acetate. Protein and reservoir solution was mixed 1:1 on a coverslip and allowed to equilibrate with the reservoir solution via the hanging drop vapor diffusion method. Hexagon-shaped crystals appeared in 1 d. The crystals were placed in a cryoprotectant solution containing 0.1 M MES pH 6.5, 1 mM 2OG, and 20% glycerol and flash-frozen with liquid nitrogen. Crystals diffracted in the $P32_1$ space-group with four monomers in the asymmetric unit. The final model contains resides 1-273 in chain A, 1-273 in chain B, 1-273 in chain C, 1-273 in chain D, 8 formate ions, 1 Fe(II) atom, 2 NSL molecules, and 45 water molecules. The final model does not contain rotamer or Ramachandran outliers. An overall clash score of 6.00 is reported for the final model.

*SadA D157S • 2OG • NSL • Fe(II)*

Protein solution was prepared anaerobically with 10 mg/mL enzyme, 1 eq. ferrous ammonium sulfate, 5 eq. 2OG, and 1 eq. NSL. Reservoir solution was prepared with 0.1 M MES pH 6.5, 3.5 M sodium formate, and 0.05 M praseodymium (III) acetate. Protein and reservoir solution was mixed 1:1 on a coverslip; the protein-reservoir drop was then streaked with SadA_B (SadA homolog) crystal seeds and allowed to equilibrate with the reservoir solution via the hanging drop vapor diffusion method. Hexagon-shaped crystals appeared in 1 d. The crystals were placed in a cryoprotectant solution containing 0.1 M MES pH 6.5, 5 eq. 2OG, 5 eq. NSL, and 20% glycerol and flash-frozen with liquid nitrogen.

Crystals diffracted in the $P32_1$ space-group with four monomers in the asymmetric unit. The final model contains 1-273 residues in chain A, 1-273 residues in chain B, 1-273 residues in chain C, 1-273 resides in chain D, 4 Fe(II) atoms, 10 formate ions, 4 NSI molecules, and 132 water molecules. 96.86% of modeled residues are Ramachandran-preferred or allowed. No rotamer outliers are in the final model. An overall clash score of 6.75 is reported for the final model (Molprobity).

*SadA D157G • 2OG • NSI • Fe(II) • Cl*

Protein solution was prepared anaerobically with 10 mg/mL enzyme, 1 eq. ferrous ammonium sulfate, 5 eq. 2OG, and 1 eq. NSI. Reservoir solution was prepared with 0.1 M MES pH 6.5, 3.5 M sodium formate, and 0.05 M praseodymium (III) acetate. Protein and reservoir solution was mixed 1:1 on a coverslip and allowed to equilibrate with the reservoir solution via the hanging drop vapor diffusion method. Hexagon-shaped crystals appeared in 1 d. The crystals were placed in a cryoprotectant solution containing 0.1 M MES pH 6.5, 1 mM 2OG, and 20% glycerol and flash-frozen with liquid nitrogen. Crystals diffracted in the $P32_1$ space-group with four monomers in the asymmetric unit. The final model contains 1-273 residues in chain A, 1-273 residues in chain B, 1-273 residues in chain C, 1-273 resides in chain D, 4 Fe(II) atoms, 11 formate ions, 4 NSI molecules, 4 chloride ions, and 287 water molecules. All modeled residues are Ramachandran-preferred or allowed. No rotamer outliers are in the final model. An overall clash score of 4.06 is reported for the final model (Molprobity).

# Chapter 3

## Mechanistic study of the native halogenase, BesD

## Introduction

In 2019, the Chang group at the University of California, Berkeley, outlined the discovery of a unique biosynthetic pathway found in the bacterium *Streptomyces cattleya*, which produces the terminal alkyne-containing amino acid β-ethynylserine (Bes).[3] Along the pathway, many transformations of interest in synthetic chemistry are performed, including halogen installation, alkene formation, and alkyne formation. The first proposed enzymatic step of the pathway is the halogenation of the amino acid L-lysine to form 4-chloro-L-lysine. The enzyme performing this step is BesD, which was annotated as an iron(II) and 2OG-dependent oxygenase. BesD lacks the HXD/E motif expected in hydroxylases, rather possessing an HXG motif. This substitution is conserved among previously characterized Fe(II)/2OG halogenases, where it serves an important functional role. Omission of the carboxylate ligand facilitates halide coordination. The Chang group reported further characterization of BesD in 2019 along with a variety of enzyme homologs capable of performing related but distinct transformations.[12] This characterization included a substrate-bound structure of the enzyme, providing potential insights into the catalytic mechanism (PDB: 6NIE, Figure 13). Consistent with the sequence-based predictions, the iron coordinates with H137 and H204 and chloride binds near where a carboxylate ligand would be expected in hydroxylases. Interestingly, 2OG binds bidentate to the iron in an orientation that could allow oxygen to bind and ferryl to form without the need for the rearrangement seen with WelO5.[14]

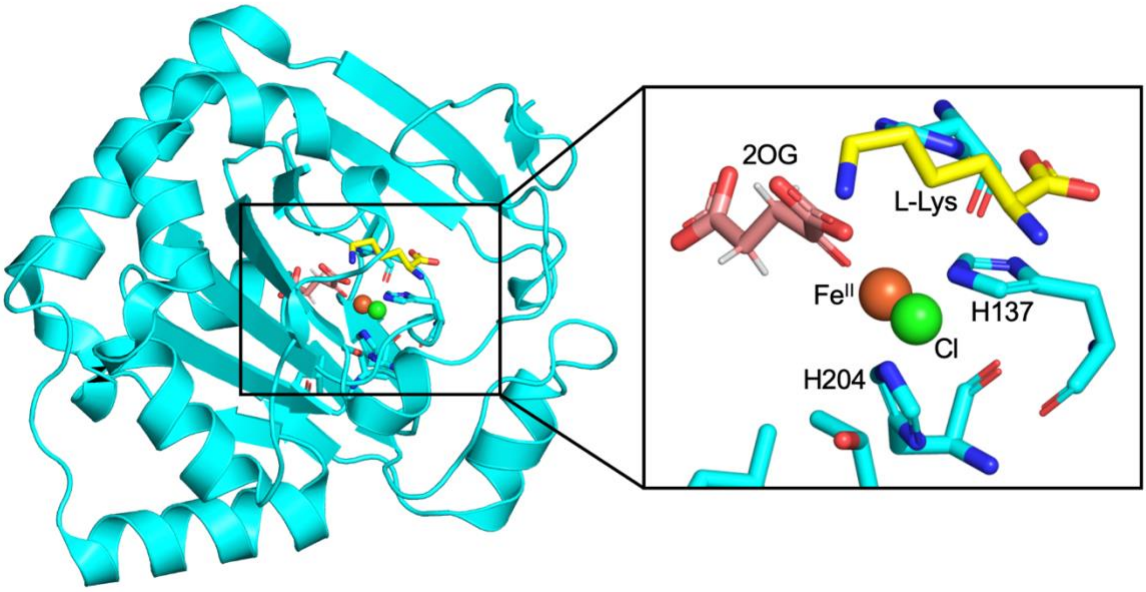


**Figure 13. Structure of BesD enzyme and active site.** The active site is similar to other Fe(II)/2OG halogenases (i.e. WelO5), with the orientation of 2OG coordination as an exception.[12,14]

BesD is particularly notable as an Fe(II)/2OG halogenase because it halogenates a simple, commercially available, and biologically relevant substrate, L-lysine. SyrB2, one of the first Fe(II)/2OG halogenases to be characterized, utilizes a carrier protein (SyrB1) to deliver its substrate, making both scientific study and biocatalytic application difficult.[13] Similarly, WelO5, which is currently the best structurally-characterized Fe(II)/2OG halogenase, utilizes a complex substrate that is not commercially available (12-epi-fischerindole U), complicating its usage.[14] As one of the first discovered Fe(II)/2OG halogenases to utilize a simple, carrier-protein-independent substrate, BesD has the potential to serve as a model halogenase from both a structural and mechanistic standpoint.

The preliminary activity characterization of BesD demonstrates that the enzyme chlorinates lysine with regioselectivity at the 4-position.[12] Minor chlorination activity has also been shown with L-ornithine when the enzyme is incubated with a cocktail of amino acids.[12] From an activity standpoint,

there is interest in understanding the scope of substrates that BesD can chlorinate. It would be of utility to biocatalytic applications to possess reactivity with multiple distinct substrates, allowing for several transformations using a single protein. From a mechanistic standpoint, understanding the common features and functionality between reactive substrates can shed light on how the enzyme interacts spatially with the substrate throughout the reaction cycle. In the solved structure of the reactant complex, we see that L-lysine carboxylate and terminal amine make several hydrogen bonding interactions with protein; thus if changes are made in the substrate structure, we may see changes in activity resulting from altered substrate binding energetics (Figure 14). For example, studies with L-ornithine - which possesses one less carbon in its side chain than L-lysine - may provide insight on how substrate binding and enzyme activity is changed with a shorter side chain. Similarly, examination of D-lysine, the stereoisomer of L-lysine, can show if reactivity and selectivity is preserved with a simple switch of the alpha carbon stereochemistry. For these reasons, examination of substrate analogs is a focus of this chapter.

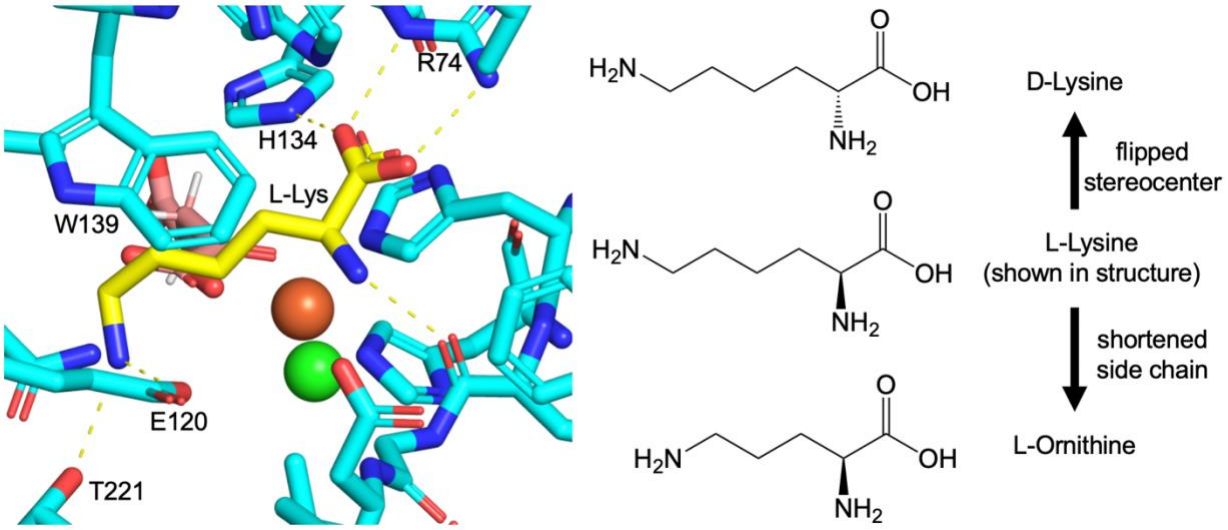


**Figure 14. Lysine binding pocket and comparison with structural analogs.** The carboxylate and terminal amine of L-lysine each make several polar contacts with the protein.[12] To probe how changes in substrate structure may affect these interactions, we use substrate analogs D-lysine and L-ornithine, which differ in stereochemistry and side chain length, respectively.

# Results and Discussion

## LC-MS Assays with Substrate Analog L-Ornithine

The activity of BesD with L-ornithine was first assessed using multi-turnover assays (Figure 15). Following quenching of the reaction, the reaction mixture was analyzed via LC-MS to detect unreacted substrate, monochlorinated product, and hydroxylated product. Monochlorinated product is detected at 167 m/z and 169 m/z (M+2), consistent with the previously published ornithine reactivity. Two peaks are present in each trace, suggesting two distinct chlorinated ornithine isomers. Hydroxylated product (149 m/z) is also observed. The source of the hydroxylated product is unclear, as non-enzymatic decay of 4-chloro-L-lysine into 4-hydroxy-L-lysine form has been reported in the initial characterization of BesD. This decay occurs via cyclization of the 4-chloro-L-lysine product into a lactone or lactam intermediate, followed by attack of water at the 4-carbon, yielding 4-hydroxy-L-lysine. This decay could also exist in the similar substrate L-ornithine, making it impossible to determine the source of the hydroxylated ornithine without further studies (i.e. isotopic labeling of the oxygen reactant). The largest fraction of detected species is unconverted L-ornithine, likely due to unproductive oxidation of 2OG and uncoupling from reaction with substrate.

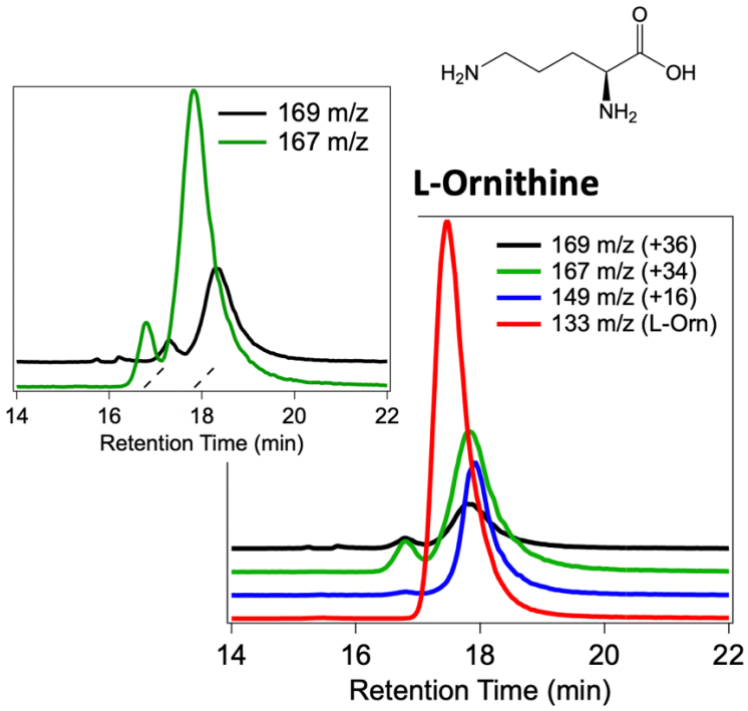


**Figure 15. BesD multiturnover activity assays with L-ornithine.** Both chlorinated and hydroxylated product is observed, with much of the substrate remaining unreacted.

To interrogate the identity of the two chlorinated products, assays were performed using deuterium isotopes of L-ornithine (Figure 16). Substitution of a deuterium for a protium slows hydrogen abstraction; thus, if deuterium is substituted at a reactive carbon, it will exhibit slowed/lesser turnover. If the carbon that is deuterated is not a reactive carbon, no difference from the original substrate will be observed as the hydrogen abstracted is still a protium. Thus, L-ornithine isotopologues can be selected to systematically rule out potential reactive carbons.

The first isotopologue, $d_2$-5,5-L-Orn, was chosen to reveal if any chemistry occurs at the 5-carbon. Multi-turnover assays with $d_2$-5,5-L-Orn were performed using the same conditions as with the original substrate, allowing for comparison of the chromatograms. The $d_2$-5,5-L-Orn reaction mixture chromatogram is essentially unchanged compared to that of the original ornithine. If the 5-carbon chloro-product were one of the two observed peaks, we would have observed one of the peaks growing and one

shrinking (or even vanishing) as the deuterated carbon center becomes kinetically favorable. Therefore, a 5-chloro product is likely not one of the major chlorinated ornithine products.

The second isotopologue, $d_4$-4,4,5,5-L-Orn, was assayed to determine chemistry at the 4-carbon. Compared to the original assay, we observed substantially less product formation, suggesting that 4-chloro-L-ornithine is a major product. Unexpectedly, however, the ratio of two peaks in the chlorinated trace remains unchanged. The consistency in peak ratio may suggest the formation of two stereoisomers, rather than two constitutional isomers. If two distinct constitutional chlorinated isomers were formed, the product ratio would be expected to shift when one of the carbons is deuterated while the other remains undeuterated. However, since the substitution of deuterium at a single carbon (4-carbon) impacts the peaks uniformly, the formation of diastereomeric products is most supported by the data.

Lastly, the isotopologue $d_7$-per-L-Orn (deuterium at 2, 3, 4, and 5 carbons) was used to assess any remaining chemistry happening at the 3-carbon or 2-carbon. We see diminished product formation with preservation of the chloro-product ratio, similar to the chromatograms observed with the previous isotopologue. As we do not see elimination or creation of any major peaks, it is unlikely that substantial chemistry is occurring at the 2 or 3 carbons.

Between the three deuterium isotopologues, the data most strongly suggests that chemistry predominately occurs at the 4-carbon of L-ornithine. The two chlorinated peaks observed are unlikely to be constitutional isomers, but rather diastereomers. If the two peaks are in fact stereoisomers, it is implied that the enzyme loses stereospecificity when using L-ornithine as substrate. As the three-dimensional configuration of ornithine bound to the active site is not known, it is uncertain how the formation of two stereoisomers is promoted. If we assume that as a non-native substrate, ornithine binds less rigidly, it may be plausible to suggest that the “floppiness” of the substrate in the active site promotes loss of stereospecificity and formation of two stereoisomers.

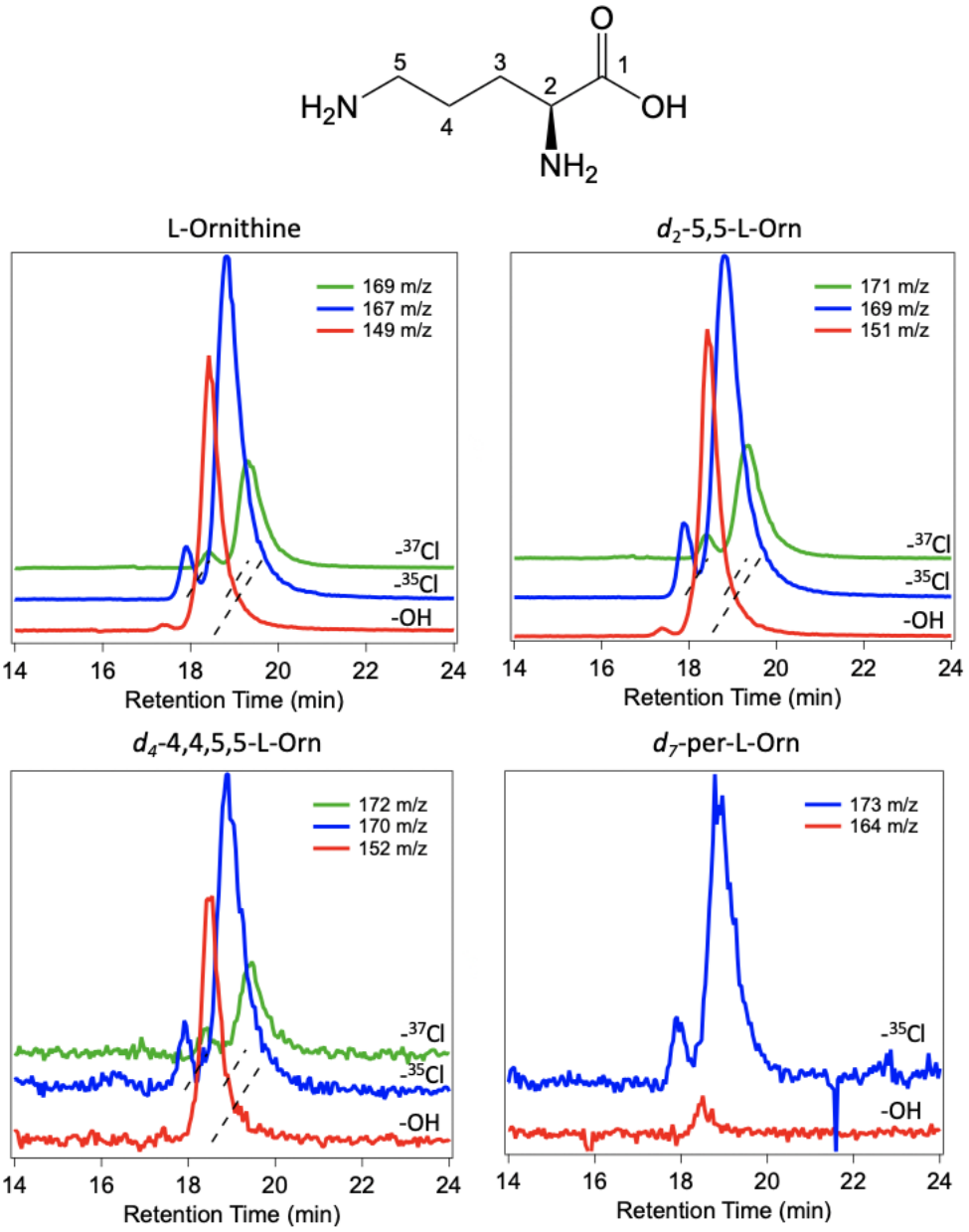


**Figure 16. BesD multiturnover activity assays with L-ornithine isotopologues.** Diminished product formation seen in the $d_4$-4,4,5,5 and $d_7$ isotopologues suggests formation of a 4-chloro-L-ornithine product.

## LC-MS Assays with Substrate Analog D-Lysine

A corresponding analysis of BesD activity with D-lysine was performed (Figure 17). The preliminary activity assay shows a small amount of chlorination activity at 181 m/z and 183 m/z (M+2). The hydroxylated product peak is far larger (163 m/z); however, the true ratio of enzymatic hydroxylation to chlorination is confounded by potential non-enzymatic decay of the chlorinated product into the hydroxylated product. Again, we observe two peaks in the chlorinated and hydroxylated product pools, bringing into question the chemical identity of the two products. Similar to with the L-ornithine, a large fraction of the substrate pool remains unconverted.

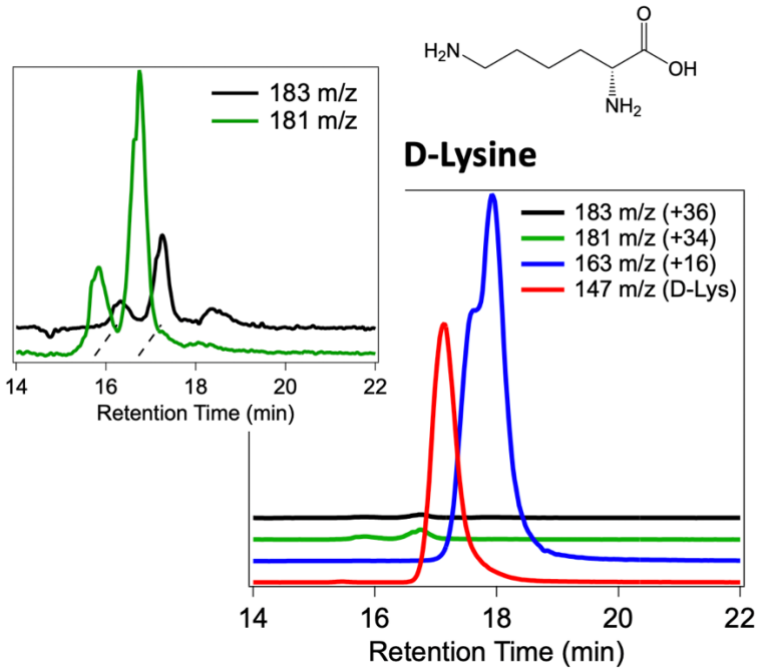


**Figure 17. BesD multiturnover activity assays with D-lysine.** Chlorinated product is detected, but the major fraction of detected products is hydroxylated. Similar to with L-ornithine, a large fraction of substrate remains unreacted.

Assays with D-Lysine isotopologues were performed to dissect which carbons are reactive centers (Figure 18). Due to the limited commercial availability of D-lysine isotopologues, only $d_4$-4,4,5,5-D-lysine was available. With this isotopologue, we can only discern whether the 4- and 5-carbon are reactive centers; however, we cannot distinguish between carbons 4 and 5. The results from the $d_4$-4,4,5,5-D-lysine assay show reduced product formation, suggesting that either the 4- or 5-carbon is reacting. Similar to the L-ornithine, two product peaks are observed, but here we cannot conclusively determine whether the two peaks correspond to the same carbon (either stereoisomeric products on the 4 or 5 carbon), or whether the two peaks correspond to different carbons (one product on the 4 and one on the 5). Synthesis of a $d_2$-5,5-D-lysine would help answer this question, but the question for now is outside the scope of this thesis.

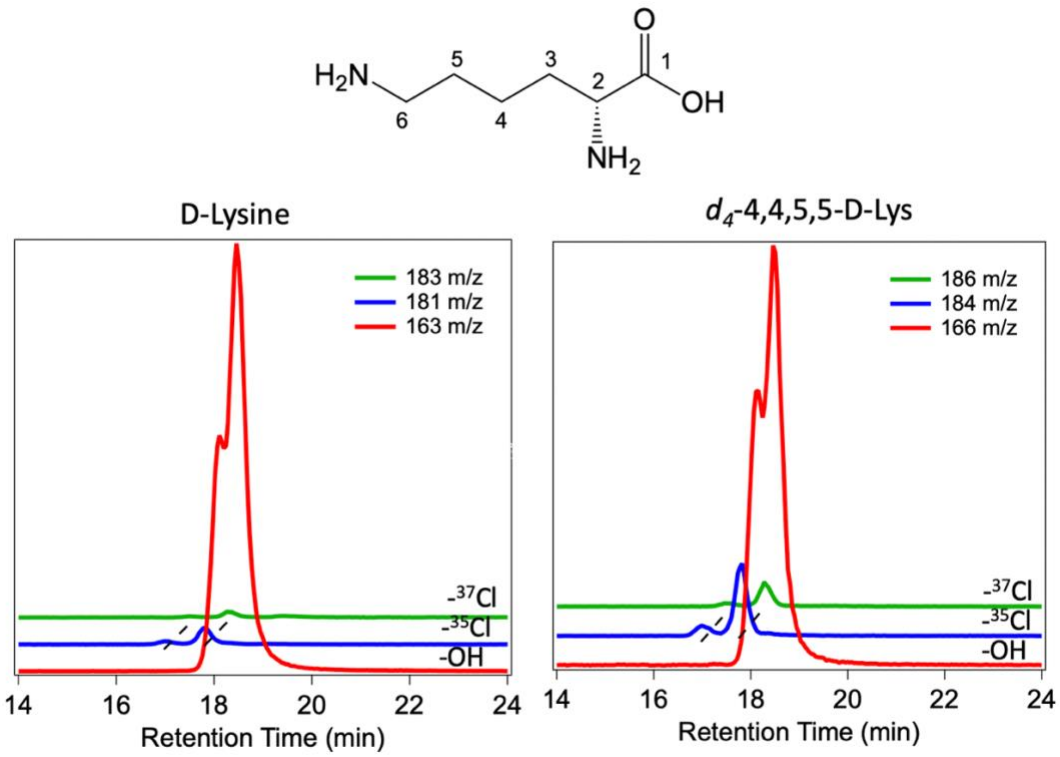


**Figure 18. BesD multiturnover activity assays with a D-lysine isotopologue.** Diminished product formation seen in the isotopologue suggests formation of either a 4-chloro or 5-chloro-D-lysine product.

## Chloride Binding Titrations with Substrate Analogs

To understand the mechanistic underpinnings for activity of BesD with its substrates, the various intermediates formed throughout the reaction cycle can be monitored. This monitoring can be accomplished in a static way, in which we stop the reaction at a certain intermediate, or in a dynamic way, in which we monitor a certain intermediate's formation and decay. However, to accomplish either, the given intermediate must be detectable. We first focus on the monitoring the Fe(II) complex prior to oxygen binding, which is detectable by UV/Vis spectroscopy (Figure 19). In the Fe(II) state, there is an observable Fe(II)→2OG metal-to-ligand charge transfer band, allowing us to probe this intermediate.[29] Furthermore, in halogenase enzymes, upon chloride binding, there is a detectable shift in the band maximum from about 495 nm to 530 nm. This shift gives us a means by which to analyze chloride binding in the Fe(II) state.

Initial investigation of this phenomenon by postdoc Jeff Slater unearthed an interesting relationship between chloride and substrate binding. If chloride is added in the Fe(II) state with no L-lysine under anoxic conditions (preventing oxygen binding), extreme concentrations are required to saturate the active site (~1.5 M NaCl). However, if chloride is added in the presence of substrate, the concentration of chloride required to saturate the active site drops dramatically. Quantitatively, the chloride dissociation constant with no substrate is 690 ± 40 mM, while it drops 300-fold to 2.3 ± 0.1 mM when just 1 mM of L-lysine is included. The chloride titrations were performed at three lysine concentrations (1 mM, 6 mM, 30 mM) to elucidate the relationship between chloride binding. The apparent chloride dissociation constant was observed to diminish with increasing lysine concentration, with chloride binding as tightly as 73.0 ± 0.8 μM when in the presence of 30 mM L-lysine. Overall, the observed apparent cooperativity between substrate and chloride binding, which has not been previously reported in Fe(II)/2OG halogenase systems, represents an interesting phenomenon that has implications for reactivity and substrate selectivity.

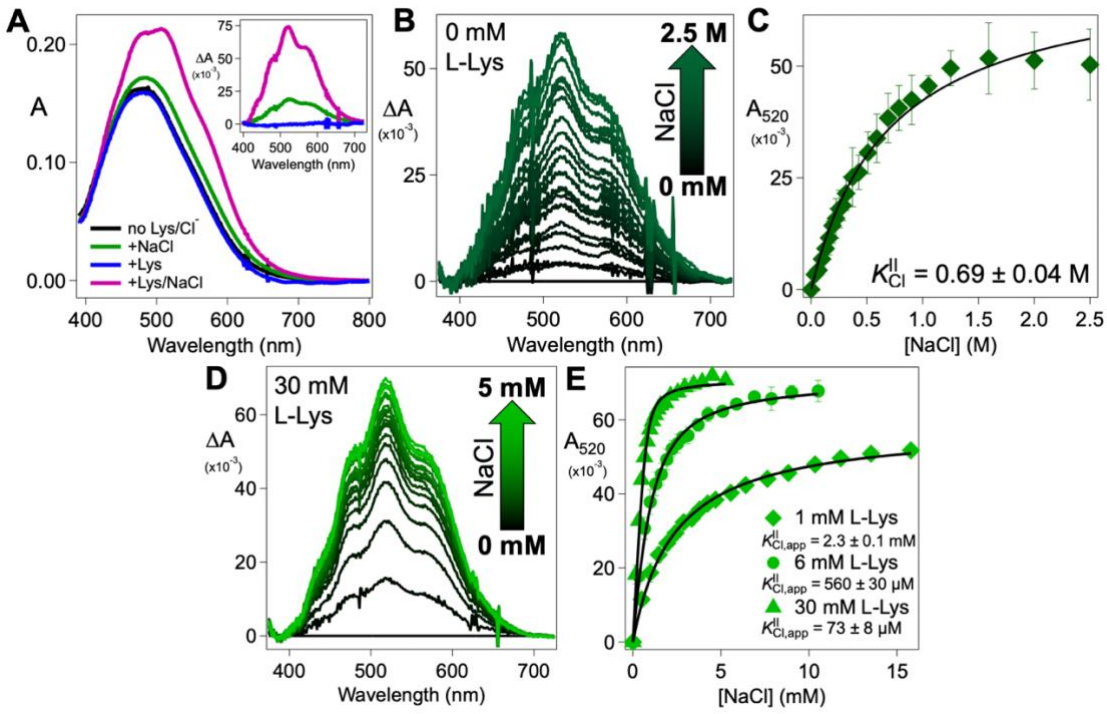


**Figure 19. Chloride and substrate binding is synergistic in BesD.** (A) A signification perturbation in the Fe(II)-2OG MLCT is only shown when both chloride and L-lysine are present, indicating cooperativity between the two species. (B) The active site can be saturated with chloride in the absence of L-lysine, but requires molar concentrations of chloride. (C) Chloride binding curve in the absence of L-lysine. (D) The chloride-induced Fe(II)-2OG MLCT perturbation occurs much more readily in the presence of 30 mM L-lysine. (E) Chloride binding curve at 1 mM, 6 mM, and 30 mM L-lysine.

To probe whether this chloride-substrate cooperativity extends to the substrate analogs, the chloride titrations were repeated with D-lysine and L-ornithine (Figure 21). The same three substrate concentrations (1 mM, 6 mM, and 30 mM) were used, and all other species (enzyme, Fe(II), 2OG) were kept at their original concentrations. Interestingly, the same cooperativity is observed in the substrate analogs, in which we see tighter observed chloride binding at higher substrate concentrations. However, the magnitude to which the substrate impacts chloride binding varies between L-lysine, D-lysine, and L-ornithine. By visual inspection, for D-lysine, the apparent chloride binding is slightly weaker than L-

lysine, but it is in the same order of magnitude. However, for L-ornithine, the apparent chloride binding is approximately 10-fold weaker.

Based on a mechanistic model derived for the Fe(II) state, the cooperativity associated with substrate binding can be extracted. Following Fe(II) and 2OG binding, either chloride or lysine can bind (with very weak affinity). Once the first species binds, the second species binds with greatly increased affinity. These binding events can be modeled as a "square scheme," and by algebraic manipulation of the equilibrium constants, the apparent chloride binding can be related to the cooperativity term (α) multiplied by the substrate dissociation constant ($K_{substrate}$) (Figure 20). This combined parameter ($\alpha K_{Substrate}$**)** quantifies the "cooperativity" of substrate binding following the initial chloride binding event, with a smaller value representing tighter binding. By fitting the three concentrations for each substrate, this parameter was determined to be 3.4 μM for L-Lys, 11 μM for D-Lys, and 68 μM L-Orn (Figure 21). To determine the cooperativity parameter, in isolation, substrate binding in the absence of substrate would need to be detected. This could be accomplished using microscale thermophoresis (MST); however, sensitivity of detection could prove problematic since D-lysine and especially L-ornithine bind weakly.

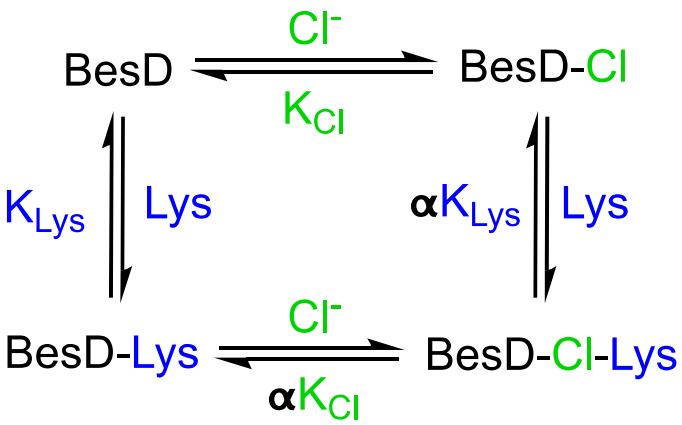


**Figure 20. Binding equilibria for L-lysine and chloride in the Fe(II) state.** The initial binding of one species followed by cooperative binding of the second forms a "square scheme." Algebraic rearrangement of equilibrium constants in this scheme allows for the determination of substrate cooperativity via chloride titration.

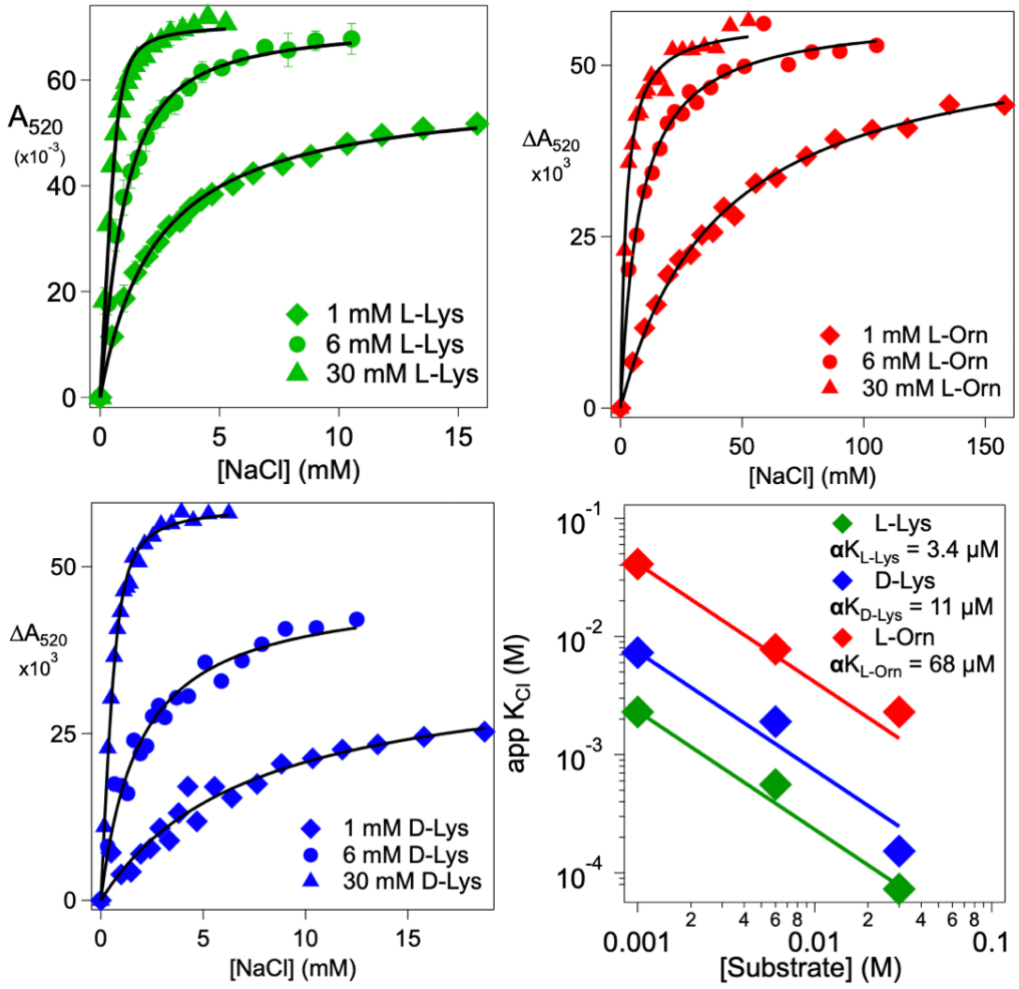


**Figure 21. Chloride binding curves for L-lysine, L-ornithine, and D-lysine.** The apparent chloride binding affinity is highest for the native substrate L-lysine, slightly weaker for D-lysine, and approximately 10 times weaker for L-ornithine. The bottom right panel shows the fitted lines from the mechanistic model and the extracted value for cooperative substrate binding.

## Ferryl Intermediate Monitoring with Stopped-Flow Absorption Spectroscopy

With this information regarding chloride dependency of substrate binding, we can dynamically monitor a later intermediate, the Fe(IV)-oxo (ferryl), to observe effects of chloride concentration on the formation and decay of this critical intermediate.[30] We use stopped-flow absorption spectroscopy to accomplish this goal by monitoring the ferryl absorbance at 318 nm. Stopped-flow experiments were performed for all substrates and isotopologues at varying chloride concentrations to see how the reaction kinetics are altered.

The L-lysine, $d_4$-L-lysine, D-lysine, and $d_4$-4,4,5,5-D-lysine data all follow similar trends (Figure 22). At high chloride concentration (1 or 1.5 M), it is shown that each substrate and its corresponding isotopologue triggers ferryl formation at a similar rate, and the rate of ferryl decay is consistent with the expected kinetic isotope effect (KIE) (i.e. deuterium will be abstracted slower and thus ferryl decays at a slower rate). Comparing results at high chloride concentration to low chloride concentration allows for examination of the role of chloride in the ferryl state. Deuterated substrates at low chloride concentration exhibit faster ferryl decay than deuterated substrates at high chloride, perhaps suggesting that high chloride leads to substrate retention and attempted (slow) hydrogen abstraction in the active site, while low chloride leads to the substrate "falling out" of the active site. In contrast, with protiated substrates, we see faster ferryl decay at higher chloride. This may suggest that hydrogen (protium) abstraction occurs in both chloride concentrations, but the increased chloride facilitates improve substrate retention and thus speeds up the reaction.

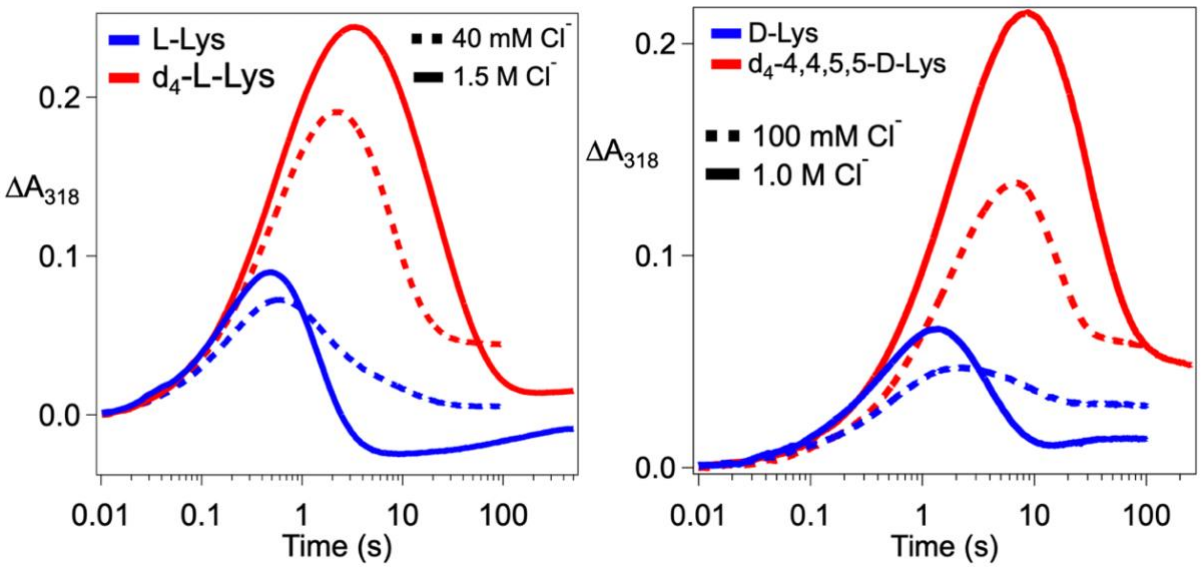


**Figure 22. Stopped-flow absorption spectroscopy with L-lysine and D-lysine.** Observed differences with isotopologues is consistent with expected slowing seen with deuterium abstraction. Chloride concentration also alters the decay rate, retaining the substrate in the active site.

Stopped-flow data with L-ornithine provides more conclusive data surrounding the role of chloride throughout the reaction cycle (Figure 23). The trace for all isotopologues is identical at low (100 mM) chloride, suggesting that ferryl formation and decay occurs at the same rate for all species. Thus, the data strongly suggests that no chemistry is performed in this condition because the deuteration of active sites would alter the rate of ferryl decay (via KIE). Since no chemistry is performed but the ferryl still decays, the results suggest a model in which the substrate "falls out" of the active site prior to hydrogen abstraction and unproductive oxidation occurs. The unproductive oxidation is also suggested by the leveling out of the traces high above baseline, suggesting poor coupling and substantial ferric formation. At 1 M NaCl, we see the traces diverge, in which all substrates trigger ferryl formation at the same rate but exhibit ferryl decay at a rate consistent with the hydrogen species (i.e. protium or deuterium). This divergence suggests that productive turnover occurs at 1 M chloride. Furthermore, the traces return much

closer to baseline, demonstrating significantly reduced ferric formation compared to the 100 mM data. A summary of this chloride-induced change in reaction outcome is shown in Figure 24.

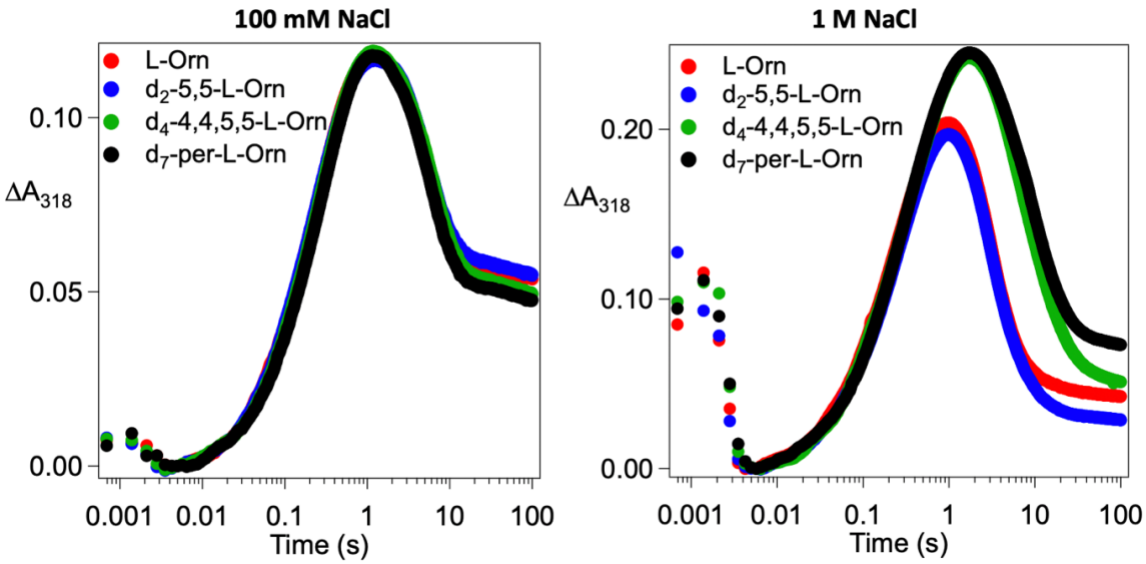


**Figure 23. Stopped-flow absorption spectroscopy with L-ornithine and isotopologues.** At 100 mM chloride, substrate-triggered ferryl formation occurs, but no productive turnover is observed. At 1 M chloride, the traces diverge according to hydrogen isotope identity suggesting that higher chloride facilitates productive turnover.

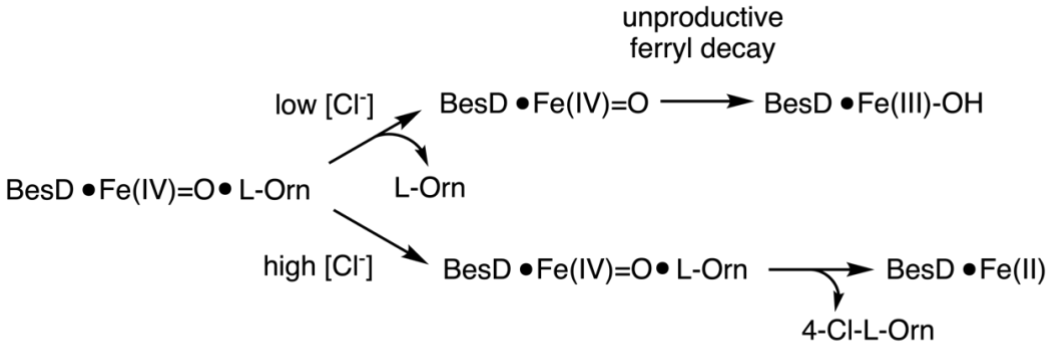


**Figure 24. Chloride partitioning of reaction outcome with L-ornithine.** At low chloride concentrations (~100 mM), unproductive ferryl decay occurs, indicated by the indistinguishable stopped-flow traces between all isotopologues. At high chloride concentrations (~ 1M), the chlorinated product is formed, shown by the observable KIE in the stopped-flow traces.

## Discussion and Broader Impacts

The stopped-flow data demonstrates that the chloride dependency of BesD exists in several critical intermediates, including the Fe(IV)-oxo state. Based on the chloride titration data, we also observe cooperativity between chloride and substrate in the Fe(II) state, suggesting a mechanistic role for the anion during formation of the initial reaction complex. This chloride dependency seen throughout the reaction cycle, summarized in Figure 25, has not been previously observed in halogenases, and could have an underlying structural basis. These results shed light on the value of further crystallographic efforts with native halogenases to understand the reasons for persistent chloride dependency. Though a crystallographic snapshot of the Fe(II) complex has been captured for BesD, obtaining structures using vanadyl as a mimic for the ferryl state would further elucidate the experimental observations in this chapter. Since the chloride ion is understood to play a fundamental role in many of these steps, anomalous diffraction data with bromide would be critical in visualizing the anion movement and dynamics.

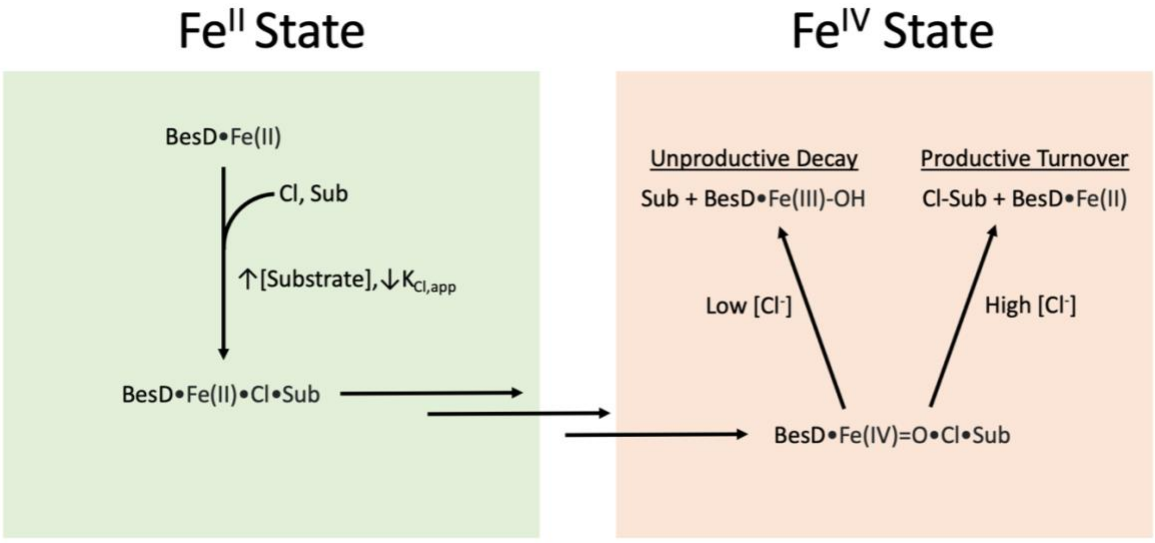


**Figure 25. Summary of chloride dependence in Fe(II) and Fe(IV) states.** In the iron(II) state, increased substrate lowers the apparent binding constant of chloride, suggesting cooperativity between the two species. In the iron(IV) state, chloride concentration is responsible for partitioning between the unproductive decay and productive turnover pathways.

The chloride dependency of the Fe(IV)-oxo state also has some interesting implications for BesD reactivity. We may often think of enzymatic reactions as being "locked in" following substrate binding; however, our data shows that substrate can efficiently bind and trigger complete ferryl formation but then dissociate and lead to unproductive decay. This generation of a reactive iron(IV)-oxo species without subsequent hydrogen abstraction could also be useful experimentally. For example, if we know that a given substrate will trigger ferryl formation but will fall out of the active site, can we introduce a less-reactive substrate during the lifetime of the ferryl and obtain chlorinated product? Such an experiment could be rationalized using the low chloride ornithine stopped-flow data reported in this chapter.

The results shown with D-lysine and L-ornithine also motivate further investigation of what substrate features perturb or alter enzymatic activity. Here, we show that the two substrate analogs bind weaker relative to L-lysine, but also see that reactivity likely stays on the 4-carbon in both substrate analogs. In substrate analogs used with previous Fe(II)/2OG enzymes, significantly more dramatic changes in reactivity have been observed. For example, in the L-arginine hydroxylase VioC, use of D-arginine as substrate promotes hydrogen abstraction from the 2-carbon instead of the 3-carbon, ultimately leading to amine desaturation rather than hydroxylation.[31] Thus, it is interesting that substitution of D-lysine or even L-ornithine for L-lysine as substrate in BesD yields a somewhat minor, if any, difference in reactivity. If it is true that the two product peaks seen in the activity assays with D-lysine and L-ornithine are diastereomeric chloro-products, it might suggest a model in which the substrate analogs bind in roughly the same position as L-lysine to facilitate C4 chemistry, but with weaker and less rigid substrate binding to allow loss of stereospecificity. Overall, these results demonstrate uncertain determinants of substrate reactivity, motivating further investigation with structural and kinetic studies.

# Materials and Methods

*BesD cloning, overexpression, and purification.*

The *Streptomyces lavenduligriseus* BesD gene, originally in a pET16-His-PrecissionCutSite-IMPDH vector, was isolated via NdeI/XhoI (NEB) double digest. The excised gene was cloned into a pET26b expression vector and rendered tagless with a stop codon preceding the vector C-terminus His tag. The construct was verified by Sanger sequencing at the Penn State Molecular Core Facility. The BesD gene sequence is below with start/stop codons bolded:

**ATG**AGCAGCAATGGGCAGGAAAGCACCGTCGTCAATCCTCTGGAGCAGGGCGCACTGCGCC
GTATGGCGCATCACTACCACCGGTACGGCATCGCCACCGTCACCGATCTGATTCGGGAAGAC
GTCCGCAAAAACGTGCGGGCGGAGGCGGACCGGCTGCTGGAGAAATACGCCGAGCGGCGTG
ATCTCCGCCTCCAGACCACCGGATACACCCGCCGCTCGATGTCCGTGGTGCAGAGCGAGACG
ATCGCGGGCAACAGCGAGCTGGTCACCTCGATCTACGCGAATCCGGAACTGCTCGGCGCGCT
GGAGCGCATAGCCGGCGAGAAACTGCACCCCTGCCCCAAGGCCGACGAGGAATTCCTCATC
ACCCGGCAGGAACGGAGCGGGGACACGCACGGCTGGCACTGGGGCGATTTCAGCTTCGCCC
TCATCTGGGTGCTCCAGGCCCCGCCCATCGACATCGGCGGCATGCTCCAGTGCGTACCGCAC
ACGGAGTGGGACAAGTCCGATCCGCGGATCCACCAGTATCTCGTCGACAATCCCATCCACAC
GTACCACTTCCAGTCGGGCGACGTGTATTTCCTGCGCACCGACACCACGCTCCACCGCACGG
TCCCGCTGCGCGAGGACACCACCCGCATCATCCTGAACATGACCTGGGCGGGCGAGCGGGA
CCTGCGGCGCGAGCTCAAGGGCGACGACCGCTGGTGGGAGGACGCCGACGTGCCGGCAGCC
GCTGCACTGGATGAC**TGA**

The pET26b BesD construct was transformed into BL21 *E. coli* cells via heat-shock protocol. A single plated colony was used to inoculate a starter culture of LB medium containing 70 ug/mL kanamycin and grown for 16-18 hours at 37 C at 200 RPM. 1 L culture flasks containing LB medium and kanamycin were inoculated with 10 mL starter culture and grown at 37 C and 200 RPM until reaching $OD_{600}$ of 1-1.2. Culture flasks were cooled on ice for 30 min before induction with IPTG (0.25 mM).

Following induction, flasks were shaken at 200 RPM at 18 C. Cells were harvested by centrifugation at 5000 XG and flash-frozen in liquid nitrogen.

Cell paste was resuspended in 5 mL/g lysis buffer containing 100 mM HEPES, pH 7.5 and ~0.1 g lysozyme and DNase I. Resuspended cells were sonicated at 50% amplitude for 7 min (10 s on, 30 s off). Cell lysate was diluted 1:1 with saturated ammonium sulfate solution and incubated for 1 hr at 4 C. Following incubation, lysate was centrifuged at 22,000 XG for 25 min. The supernatant was decanted and diluted 1:1 with 100 mM HEPES, pH 7.5. Lysate supernatant was then concentrated using a 10 kDa MWCO concentrator tube to facilitate ease of downstream purification methods. The concentrated lysate was dialyzed against 100 mM HEPES, pH 7.5 overnight to remove ammonium sulfate.

The dialyzed lysate was concentrated to <100 mL and loaded onto a Q anion exchange column (26/100, 600 mL Resin) connected to an AKTA FPLC system (GE Healthcare). Gradient elution was performed from 0-50% buffer A to buffer B (100 mM HEPES, 1 M $MgSO_4$, pH 7.5) with a subsequent wash of 100% buffer B. Protein-containing fractions were pooled, concentrated, and dialyzed against 5 mM EDTA and 100 mM HEPES, pH 7.5 for >4 hours. Two additional dialysis steps were performed with the same buffers but in the absence of EDTA. Protein purity was verified by SDS-PAGE and protein concentration calculated by absorbance at 280 nm (e = 50,420 1/M-cm).

*Substrate dechlorination.*

Since commercially available substrate salts contain HCl as a counter ion, chloride must be removed to avoid confounding chloride concentration in experiments. The substrate salt was dissolved in 100 mM HEPES and pH-adjusted to pH 6-8 with 1 M NaOH. A 5 mL FF Q-column (Cytiva) was rinsed with 25 mL of 1 M ammonium acetate, pH 6.5 to outcompete the resin-bound chloride ions. The column was then washed with 25 mL water. The substrate solution was loaded onto the column and eluted with 10 mL $H_2O$. As the substrate is loaded onto the column, the chloride counter ions will bind to the resin while the positively charged substrate flows through. The collected eluate was flash frozen in liquid nitrogen and lyophilized for 1 d. The solid was resuspended in water. Sufficient dechlorination was

verified by adding a high concentration of the stock to the Fe(II) quaternary complex; no shift in the Fe(II)-2OG MLCT should be observed.

*LC-MS activity assays*.

Reactions contain 1 mM substrate, 0.1 mM ferrous ammonium sulfate, 0.1 mM BesD, 5mM 2OG, 5 mM ascorbic acid, and 1 M NaCl. The reaction was initiated by the addition of 2OG aerobically, mixed, and allowed to proceed for 20 min. The reaction was quenched 1:1 with acetonitrile. Internal standards of a different isotopologue were added following quenching ($d_4$-L-Lys as a standard for L-Lys). Reaction products were isolated via a 10 kDa MWCO spin column. 5 uL of each reaction mixture was injected onto a SeQuant ZIC-HILIC (EMD Millipore) column and eluted via a linear gradient of 95% B to 30% B over 25 min followed by a linear gradient of 30% B to 95% B over 5 min at a flow rate of 0.2 mL min (A- 10:90 MeCN:water, 10 mM ammonium formate, pH 5.0, B- 90:10 MeCN:water, 10 mM ammonium formate, pH 5.0).

*Chloride titrations.*

The Fe(II) complex was assembled with 1 mM enzyme, 10 mM 2OG, 500 μM DT, 0.72 mM ferrous ammonium sulfate, and 1-30 mM substrate in 100 mM HEPES, pH 7.5. A spectrum was taken in the absence of chloride. Aliquots of chloride were added and a spectrum was recorded following addition of each aliquot and mixing of the solution. Aliquots were added until saturation of the signal was achieved. Dilution was corrected for and the absorbance at 800 was set to zero. The spectrum baseline was corrected in MATLAB.

*Stopped-flow absorption spectroscopy*.

Stopped-flow experiments were performed on an Applied Photophysics Ltd. SX-20 stopped-flow spectrophotometer. Reactions were carried out at 5 C in a single-mixing configuration with 1 cm pathlength and photomultiplier tube detector. Reactions were performed with 0.2 mM Fe(II), 0.275 mM enzyme, 5 mM substrate, 5 mM 2OG, and 0.18 mM $O_2$ (using $O_2$ saturated buffer). Wavelengths were selected from the broadband light source before the reaction cell with a monochromator.

# Appendix A

**Table 1. Crystallographic data collection and refinement statistics for SadA**

| | *SadA* (NSL bound) | *SadA* (NSI bound) | *SadA D157S* (NSL bound) | *SadA D157G* (NSI bound) |
|---|---|---|---|---|
| **Data collection** | | | | |
| Space group | *P 31 2 1* | *P 31 2 1* | *P 31 2 1* | *P 31 2 1* |
| Wavelength (Å) | 0.9787 | 0.9786 | 0.9786 | 1.0332 |
| Cell dimensions | | | | |
| *a*, *b*, *c* (Å) | 176.12<br>176.12<br>108.48 | 175.86<br>175.86<br>107.46 | 175.04<br>175.04<br>107.02 | 175.18<br>175.18<br>107.06 |
| α, β, γ (°) | 90.0, 90.0, 120 | 90.0, 90.0, 120 | 90.0, 90.0, 120 | 90.0, 90.0, 120 |
| Resolution (Å) | 50.00 - 2.72 (2.82 - 2.72) | 50.00 – 2.63 (2.72 – 2.63) | 50.00 – 2.76 (2.86 – 2.76) | 50.00 – 2.33 (2.41 – 2.33) |
| $R_{merge}$ | 0.102 (0.000) | 0.129 (1.303) | 0.131 (1.362) | 0.112 (1.714) |
| $R_{pim}$ | 0.039 (0.435) | 0.032 (0.322) | 0.040 (0.406) | 0.029 (0.461) |
| $I / \sigma I$ | 1.93 (19.1) | 2.33 (26.6) | 1.91 (20.9) | 27.2 (1.8) |
| $CC_{1/2}$ | 0.687 | (0.716) | (0.768) | (0.704) |
| Completeness (%) | 100.0 | 100.0 | 100.0 | 99.9 |
| Redundancy | 7.2 (6.9) | 16.7 (16.3) | 10.9 (11.2) | 14.4 (13.4) |
| | | | | |
| **Refinement** | | | | |
| Resolution (Å) | 2.72 | 2.63 | 2.76 | 2.33 |
| No. reflections | 50,627 | 55,609 | 46,226 | 78303 |
| $R_{work}$ / $R_{free}$ | 0.2236/0.2644 | 0.2183/0.2585 | 0.2307/0.2735 | 0.2211/0.2490 |
| No. atoms | 8929 | 8861 | 8726 | 9000 |
| Protein | 8764 | 8695 | 8624 | 8672 |
| Ligand/ion | 109 | 34 | 57 | 41 |
| Water | 56 | 132 | 45 | 287 |
| *B*-factors | 51.11 | 48.54 | 49.05 | 39.04 |
| Protein | 51.20 | 48.77 | 49.10 | 39.15 |
| Ligand/ion | 51.83 | 53.24 | 52.99 | 47.40 |
| Water | 35.66 | 32.52 | 35.59 | 34.44 |
| R.m.s. deviations | | | | |
| Bond lengths (Å) | 0.010 | 0.0010 | 0.005 | 0.006 |
| Bond angles (°) | 1.27 | 1.36 | 1.00 | 1.11 |
| Molprobity clashscore | 6.89 ($100^{th}$ percentile) | 6.75 ($100^{th}$ percentile) | 6.00 | 4.06 ($100^{th}$ percentile) |
| Rotamer outliers (%) | 0.00 | 0.00 | 0.00 | 0.00 |
| Ramachandran favored (%) | 97.73 | 96.86 | 98.34 | 98.89 |
| PDB accession code | | | | |

*Values in parentheses are for highest-resolution shell.

# References


1. Martinez S, Hausinger RP. Catalytic Mechanisms of Fe(II)- and 2-Oxoglutarate-dependent Oxygenases. J Biol Chem. 2015 Aug 21;290(34):20702-20711. doi: 10.1074/jbc.R115.648691. Epub 2015 Jul 7. PMID: 26152721; PMCID: PMC4543632.
2. Podgorsek A, Zupan M, Iskra J. Oxidative halogenation with "green" oxidants: oxygen and hydrogen peroxide. Angew Chem Int Ed Engl. 2009;48(45):8424-50. doi: 10.1002/anie.200901223. PMID: 19827067.
3. Marchand JA, Neugebauer ME, Ing MC, Lin CI, Pelton JG, Chang MCY. Discovery of a pathway for terminal-alkyne amino acid biosynthesis. Nature. 2019 Mar;567(7748):420-424. doi: 10.1038/s41586-019-1020-y. Epub 2019 Mar 13. PMID: 30867596.
4. Herr CQ, Hausinger RP. Amazing Diversity in Biochemical Roles of Fe(II)/2-Oxoglutarate Oxygenases. Trends Biochem Sci. 2018 Jul;43(7):517-532. doi: 10.1016/j.tibs.2018.04.002. Epub 2018 Apr 27. PMID: 29709390; PMCID: PMC6014900.
5. Jr, Bollinger, & Chang, Wei-Chen & Matthews, Megan & Martinie, Ryan & Boal, Amie & Krebs, Carsten. (2015). Mechanisms of 2-oxoglutarate-dependent oxygenases: The hydroxylation paradigm and beyond. 10.1039/9781782621959-00095.
6. Li D, Guo B, Wu H, Tan L, Lu Q. TET Family of Dioxygenases: Crucial Roles and Underlying Mechanisms. Cytogenet Genome Res. 2015;146(3):171-80. doi: 10.1159/000438853. Epub 2015 Aug 21. PMID: 26302812.
7. Stolze IP, Mole DR, Ratcliffe PJ. Regulation of HIF: prolyl hydroxylases. Novartis Found Symp. 2006;272:15-25; discussion 25-36. PMID: 16686427.
8. Grzyska PK, Ryle MJ, Monterosso GR, Liu J, Ballou DP, Hausinger RP. Steady-state and transient kinetic analyses of taurine/alpha-ketoglutarate dioxygenase: effects of oxygen concentration, alternative sulfonates, and active-site variants on the FeIV-oxo intermediate. Biochemistry. 2005 Mar 15;44(10):3845-55. doi: 10.1021/bi048746n. PMID: 15751960.
9. Mitchell AJ, Dunham NP, Martinie RJ, Bergman JA, Pollock CJ, Hu K, Allen BD, Chang WC, Silakov A, Bollinger JM Jr, Krebs C, Boal AK. Visualizing the Reaction Cycle in an Iron(II)- and 2-(Oxo)-glutarate-Dependent Hydroxylase. J Am Chem Soc. 2017 Oct 4;139(39):13830-13836. doi: 10.1021/jacs.7b07374. Epub 2017 Sep 20. PMID: 28823155; PMCID: PMC5852378.
10. Ryle MJ, Koehntop KD, Liu A, Que L Jr, Hausinger RP. Interconversion of two oxidized forms of taurine/alpha-ketoglutarate dioxygenase, a non-heme iron hydroxylase: evidence for bicarbonate binding. Proc Natl Acad Sci U S A. 2003 Apr 1;100(7):3790-5. doi: 10.1073/pnas.0636740100. Epub 2003 Mar 17. PMID: 12642663; PMCID: PMC153000.
11. Pan J, Wenger ES, Matthews ML, Pollock CJ, Bhardwaj M, Kim AJ, Allen BD, Grossman RB, Krebs C, Bollinger JM Jr. Evidence for Modulation of Oxygen Rebound Rate in Control of Outcome by Iron(II)- and 2-Oxoglutarate-Dependent Oxygenases. J Am Chem Soc. 2019 Sep 25;141(38):15153-15165. doi: 10.1021/jacs.9b06689. Epub 2019 Sep 16. PMID: 31475820; PMCID: PMC6900985.
12. Neugebauer ME, Sumida KH, Pelton JG, McMurry JL, Marchand JA, Chang MCY. A family of radical halogenases for the engineering of amino-acid-based products. Nat Chem Biol. 2019 Oct;15(10):1009-1016. doi: 10.1038/s41589-019-0355-x. Epub 2019 Sep 23. PMID: 31548692.

13. Vaillancourt FH, Yin J, Walsh CT. SyrB2 in syringomycin E biosynthesis is a nonheme FeII alpha-ketoglutarate- and O2-dependent halogenase. Proc Natl Acad Sci U S A. 2005 Jul 19;102(29):10111-6. doi: 10.1073/pnas.0504412102. Epub 2005 Jul 7. PMID: 16002467; PMCID: PMC1177402.
14. Mitchell AJ, Zhu Q, Maggiolo AO, Ananth NR, Hillwig ML, Liu X, Boal AK. Structural basis for halogenation by iron- and 2-oxo-glutarate-dependent enzyme WelO5. Nat Chem Biol. 2016 Aug;12(8):636-40. doi: 10.1038/nchembio.2112. Epub 2016 Jun 27. PMID: 27348090; PMCID: PMC5391150.
15. Hegg EL, Que L Jr. The 2-His-1-carboxylate facial triad--an emerging structural motif in mononuclear non-heme iron(II) enzymes. Eur J Biochem. 1997 Dec 15;250(3):625-9. doi: 10.1111/j.1432-1033.1997.t01-1-00625.x. PMID: 9461283.
16. Pavel EG, Kitajima N, Solomon EI. Magnetic Circular Dichroism Spectroscopic Studies of Mononuclear Non-Heme Ferrous Model Complexes. Correlation of Excited- and Ground-State Electronic Structure with Geometry. J Am Chem Soc. 1998.
17. Price JC, Barr EW, Tirupati B, Bollinger JM Jr, Krebs C. The first direct characterization of a high-valent iron intermediate in the reaction of an alpha-ketoglutarate-dependent dioxygenase: a high-spin FeIV complex in taurine/alpha-ketoglutarate dioxygenase (TauD) from Escherichia coli. Biochemistry. 2003 Jun 24;42(24):7497-508. doi: 10.1021/bi030011f. Erratum in: Biochemistry. 2004 Feb 3;43(4):1134. PMID: 12809506.
18. Riggs-Gelasco PJ, Price JC, Guyer RB, Brehm JH, Barr EW, Bollinger JM Jr, Krebs C. EXAFS spectroscopic evidence for an Fe=O unit in the Fe(IV) intermediate observed during oxygen activation by taurine:alpha-ketoglutarate dioxygenase. J Am Chem Soc. 2004 Jul 7;126(26):8108-9. doi: 10.1021/ja048255q. PMID: 15225039.
19. Proshlyakov DA, Henshaw TF, Monterosso GR, Ryle MJ, Hausinger RP. Direct detection of oxygen intermediates in the non-heme Fe enzyme taurine/alpha-ketoglutarate dioxygenase. J Am Chem Soc. 2004 Feb 4;126(4):1022-3. doi: 10.1021/ja039113j. PMID: 14746461.
20. Price JC, Barr EW, Glass TE, Krebs C, Bollinger JM Jr. Evidence for hydrogen abstraction from C1 of taurine by the high-spin Fe(IV) intermediate detected during oxygen activation by taurine:alpha-ketoglutarate dioxygenase (TauD). J Am Chem Soc. 2003 Oct 29;125(43):13008-9. doi: 10.1021/ja037400h. PMID: 14570457.
21. J. T. Groves, Key elements of the chemistry of cytochrome P-450: The oxygen rebound mechanism. *J. Chem. Ed.*, 1985, 62, 928–931.
22. Mitchell AJ, Dunham NP, Bergman JA, Wang B, Zhu Q, Chang WC, Liu X, Boal AK. Structure-Guided Reprogramming of a Hydroxylase To Halogenate Its Small Molecule Substrate. Biochemistry. 2017 Jan 24;56(3):441-444. doi: 10.1021/acs.biochem.6b01173. Epub 2017 Jan 11. PMID: 28029241; PMCID: PMC5852377.
23. Rivera Pomales, P. UNDERSTANDING THE STRUCTURAL BASIS FOR MECHANISM IN TWO DIFFERENT IRON-DEPENDENT OXYGENASE SUPERFAMILIES. The Pennsylvania State University. 2021.
24. Hein, C. D., Liu, X. M., & Wang, D. (2008). Click chemistry, a powerful tool for pharmaceutical sciences. *Pharmaceutical research*, *25*(10), 2216–2 Relevant Compound. Angew Chem Int Ed Engl. 2019 Dec 16;58(51):18535-18539.

25. Arnold FH. Directed Evolution: Bringing New Chemistry to Life. Angew Chem Int Ed Engl. 2018 Apr 9;57(16):4143-4148.
26. Dunham NP, Arnold FH. Nature's Machinery, Repurposed: Expanding the Repertoire of Iron-Dependent Oxygenases. ACS Catal. 2020 Oct 16;10(20):12239-12255.
27. Hayashi T, Ligibel M, Sager E, Voss M, Hunziker J, Schroer K, Snajdrova R, Buller R. Evolved Aliphatic Halogenases Enable Regiocomplementary C-H Functionalization of a Pharmaceutically Relevant Compound. Angew Chem Int Ed Engl. 2019 Dec 16;58(51):18535-18539.
28. Neugebauer ME, Kissman EN, Marchand JA, Pelton JG, Sambold NA, Millar DC, Chang MCY. Reaction pathway engineering converts a radical hydroxylase into a halogenase. Nat Chem Biol. 2022 Feb;18(2):171-179.
29. Matthews ML, Chang WC, Layne AP, Miles LA, Krebs C, Bollinger JM Jr. Direct nitration and azidation of aliphatic carbons by an iron-dependent halogenase. Nat Chem Biol. 2014 Mar;10(3):209-15.
30. Price JC, Barr EW, Hoffart LM, Krebs C, Bollinger JM Jr. Kinetic dissection of the catalytic mechanism of taurine:alpha-ketoglutarate dioxygenase (TauD) from Escherichia coli. Biochemistry. 2005 Jun 7;44(22):8138-47.
31. Dunham NP, Mitchell AJ, Del Río Pantoja JM, Krebs C, Bollinger JM Jr, Boal AK. α-Amine Desaturation of d-Arginine by the Iron(II)- and 2-(Oxo)glutarate-Dependent l-Arginine 3-Hydroxylase, VioC. Biochemistry. 2018 Nov 20;57(46):6479-6488. doi: 10.1021/acs.biochem.8b00901. Epub 2018 Nov 7. PMID: 30403469; PMCID: PMC6424487.

# ACADEMIC VITA

of Bryce Katch

## EDUCATION

**The Pennsylvania State University – Schreyer Honors College** **University Park, PA**
**B.S. Chemical Engineering | B.S. Biochemistry and Molecular Biology** Fall 2018 – Spring 2022

## RESEARCH EXPERIENCE

**Penn State Department of Chemistry** **University Park, PA**
**Undergraduate Researcher** August 2019 – Present

- Conducted research on the Fe(II)-2OG enzyme superfamily in the lab of Dr. Amie Boal
- Cloned, expressed, and purified Fe(II)-2OG enzymes for study
- Crystallized and solved structures of reactive intermediates in Fe(II)-2OG enzymes
- Performed enzymatic activity assays using liquid chromatography-mass spectrometry

**Memorial Sloan Kettering Cancer Center** **New York City, NY**
**Undergraduate Research Intern** Summer 2021

- Studied genome topology in mammalian cells in the lab of Dr. Alexandros Pertsinidis
- Constructed an automated fluidics and microscopy setup to image regulatory DNA elements
- Performed preliminary fluorescence in situ hybridization experiments to test automated setup

**Penn State Department of Chemical Engineering** **University Park, PA**
**Undergraduate Researcher** July 2020 – May 2021

- Applied control theory to examine COVID-19 mobility policies under Dr. Antonios Armaou
- Examined the pandemic in Lombardy, Italy using a compartmental epidemiological model
- Used MATLAB to determine model parameters by mixed-integer optimization

## WORK EXPERIENCE

**Penn State Department of Chemical Engineering** **University Park, PA**
**Intro to Biomolecular Engineering (CHE 340) Instructional Aide** Fall 2020

- Held weekly office hours to assist students on homework
- Generated supplemental learning resources to help students with bioengineering principles

**Graham Architectural Products** **York, PA**
**Engineering Design Intern** Summer 2019

- Created a Microsoft Excel application to model dynamic window systems saving approximately $50,000 per project in estimating and field service
- Generated mathematical models to simulate motion of window systems
- Wrote scripts in Visual Basic to automate solving of simultaneous nonlinear equations

## INVOLVEMENT

Penn State Engineering Ambassadors Spring 2020 – Present
Penn State Marching Blue Band Fall 2018 - Present
Penn State Saxophone Studio Spring 2019 - Present

## AWARDS

Barry M. Goldwater Scholarship March 2021
Evan Pugh Scholar Award March 2021